LA-UR-13-20761
Approved for public release; distribution is unlimited.

Title:	Theoretical Treatment of Pressure Gradients in One-Dimensional, Inhomogeneous, Compressible Media
Author(s):	Letellier, Bruce C.
Intended for:	Interim Work Product Report

LA-UR-13-

Approved for public release; distribution is unlimited.

Title: **Theoretical Treatment of Pressure Gradients in One-Dimensional, Inhomogeneous, Compressible Media**

Author(s): Bruce C. Letellier
Los Alamos National Laboratory

Intended for: South Texas Nuclear Operating Company
Risk-Informed Closure of GSI-191
Interim Work Product

Form 836 (7/06)

This page intentionally left blank.

CONTENTS

Page

FIGURES iv
TABLES v
ABBREVIATIONS and ACRONYMS vi
1 INTRODUCTION 1
1.1 Background 2
2 THEORY DEVELOPMENT 6
2.1 Flow Through Porous Media 7
2.1.1 Derivation of Pressure Gradient Formulas 7
2.1.1.1 Momentum Flux Within a Control Volume 8
2.1.1.2 Body Forces Acting on the Fluid 21
2.1.1.3 Surface Forces Acting on the Fluid 22
2.1.2 Modified Ergun Equation 33
2.1.3 Hydraulic Drag 37
2.1.3.1 Drag Imparted by Fluid Shear 39
2.1.3.2 Drag Imparted by Inertial Transfer 41
2.1.4 Remaining Pressure Gradient Contributions 46
2.1.5 Summary of Head-Loss Gradient Formulas 47
3 Conclusion 49
4 BIBLIOGRAPHY 50

FIGURES

Figure 2-1. Geometry of flow through a one-dimensional porous medium: (a) bulk approach and exit velocities, (b) cylindrical differential volume element, (c) internal velocity vectors penetrating a control system of fluid (dashed boundary)..... 9
Figure 2-2. Schematic function of the vertical velocity component that might exist across any horizontal plane intersecting the debris bed..... 15
Figure 2-3. Annular control volume used for derivation of shear stress in a cylindrical capillary. 25
Figure 2-4. Drag coefficients for spheres, disks, and cylinders: $A_p =$ area of particle projected on plane normal to direction of motion; $C_D =$ overall drag coefficient, dimensionless; $D_p =$ diameter of particle; $F_d =$ drag or resistance to motion of body in fluid; Re = Reynolds number, dimensionless; $u =$ relative velocity between particle and main body of fluid; $\mu =$ fluid viscosity; and $\rho =$ fluid density. (Reprinted with from Ref. 24. Copyright 1940 American Chemical Society)..... 43

TABLES

Table 1-1. Material-Quantity/Sump-Water-Volume Ratios for the ICET Tests 5
Table 1-2. Experimental Conditions in the ICET Tests[1,2] 5

ABBREVIATIONS and ACRONYMS

ASTM	American Society for Testing and Materials
cal-sil	Calcium Silicate
CAP	Calcium Phosphate
CF	Clean Fiber
CPVC	Chlorinated PolyVinyl Chloride
DAS	Data Acquisition System
ECCS	Emergency-Core-Cooling System
EDS	Energy-Dispersive Spectroscopy
ESEM	Environmental Scanning Electron Microscopy
ft	feet
g	gram(s)
gal.	gallon(s)
GSI	Generic Safety Issue
HPSI	High-Pressure Safety Injection
ICET	Integrated Chemical Effects Tests
ICP	Inductively Coupled Plasma (spectroscopy)
in.	inches
L	liter(s)
lbf	pounds force
lbm	pounds mass
LANL	Los Alamos National Laboratory
LHS	Left-Hand Side
LOCA	Loss-of-Coolant Accident
mA	milliampere(s)
mg	milligram(s)
mL	milliliter(s)
NPT	National Pipe Thread
NRC	Nuclear Regulatory Commission
$NPSH_A$	Net Positive Suction Head (available)
$NPSH_M$	Net Positive Suction Head (margin)
$NPSH_R$	Net Positive Suction Head (required)
NTU	Nephelometric Turbidity Unit
PVC	Polyvinyl Chloride
psig	Pounds force per Square Inch (Guage)
ppt	precipitate(s)
PWR	Pressurized-Water Reactor
RHR	Residual Heat Removal (system)
RHS	Right-Hand Side
RMI	Reflective Metallic Insulation
RO	Reverse Osmosis (water)
RT	Room Temperature
SEM	Scanning Electron Microscopy
U. S.	United States
UNM	University of New Mexico

1 INTRODUCTION

The purpose of the Generic Safety Issue (GSI) -191 research program sponsored by the U.S. Nuclear Regulatory Commission (NRC) was to determine if the formation, transport and accumulation of debris in a containment building following a loss-of-coolant accident (LOCA) could impede the operation of the emergency-core-cooling system (ECCS) in pressurized-water reactors (PWRs). The definition of "debris" was incrementally expanded over the course of the program to include not only thermal insulation damaged by direct jet impingement from a broken pipe, but also the latent dust and dirt that may be present in containment, and most recently, any adverse chemical products that might arise from the unique combination of spray additives, structural materials, and damaged insulation and coatings that will be present in the post-LOCA accident environment. The Integrated Chemical Effects Test (ICET[1]) program was initiated by the NRC and conducted at the University of New Mexico (UNM) under the direction of Los Alamos National Laboratory (LANL) to study the possible formation of chemical products in prototypical containment conditions (Refs. 3, 5-8).

One primary objective of the ICET program was to identify the formation in a representative post-LOCA accident environment of any chemical products that might adversely affect the flow of water through the recirculation sump screen and lead to larger hydraulic pressure drops (head losses). A small-scale chemical effects study (Ref. 17) had previously demonstrated that chemical products associated with the corrosion of structural metals in representative containment-chemistry solutions can induce large pressure drops when deposited on fiberglass insulation debris, but no attempt was made to demonstrate that these products form naturally as part of the long-term chemical environment in the containment pool. Subsequently, the ICET series determined that a number of chemical products can be formed in a realistic containment environment over a 30-day period and that these products can be deposited on and within mats of fiberglass debris, but conversely, no attempt was made to characterize the potential head-loss characteristics of these products.

South Texas Project Nuclear Operating Company (STP) has recently initiated the Chemical Head Loss Effects (CHLE[2]) test series (Ref. 44) at UNM to examine site specific chemical product formation and to characterize composition, quantity, and morphology of any identified products for the purpose of supporting a chemical head-loss testing study. STP utilizes almost 100% fiberglass insulation to improve thermal efficiency within the plant. Latent (permanently resident) debris can contribute a small amount of additional fiber as well as dust and dirt particulates. The dominant particulate type at STP is from unqualified coatings materials that are presumed to suffer complete mechanical degradation. Because STP maximum strainer approach velocities under ECCS recirculation are very low (~0.009 ft/s), the NRC has questioned the use of traditional head-loss correlations (Ref. 43) that relate debris-bed composition and thickness to pressure drop. STP has planned additional tests to study debris accumulation and penetration through a prototypical sump-strainer module. Also, a relatively new

[1] pronounced "ice tea"
[2] pronounced "chili"

surrogate-debris preparation method (Ref. 45) is being used to separate fiberglass insulation; debris preparation has long been recognized as an important influence on head-loss behavior.

STP is planning a vertical loop head-loss test program to investigate the combined effects of (1) low bed-formation and approach velocities, (2) new fiber preparation methods, (3) high particulate-to-fiber ratios, and (4) chemical product formation. These tests will support either (a) validation of the 6224 correlation for STP conditions, (b) refinement of traditional correlations in the form of tailored fitting parameters, or (c) development of new correlations that address recognized deficiencies for treating hydraulic compression and compaction in mixed debris beds with inhomogenous composition profiles.

This report reviews the theoretical construction of traditional head-loss correlations, and expands the mathematical treatment to accommodate inhomogeneous composition profiles. The primary focus of this treatise is pressure gradients through a fixed thickness of a one-dimensional, inhomogeneous bed of mixed composition.

1.1 Background

In the event of a LOCA within a PWR containment, thermal insulation and other materials (e.g., coatings and concrete) in the vicinity of the break would be damaged, and a fraction of the debris that was formed would be transported to the emergency recirculation sump. The subject of high-pressure debris generation and waterborne transport has been studied extensively as part of safety analysis activities for both the U.S. BWR and PWR plant populations (Refs. 1, 35, 43). For four-loop plant configurations primarily insulated with fiberglass, debris volumes may exceed 2000 ft^3 for a large-break LOCA. Part of the debris reaching the sump screen would accumulate on the face, and part of the debris would pass through. Debris accumulating on the screen can form a bed that acts as a filter capable of removing particulate matter from the circulating water, thus increasing the pressure drop, or "head loss," across the screen. Excessive head loss may prevent or impede the flow of water to the ECCS and to the containment spray system, potentially degrading system performance or causing pump damage.

Containment spray systems are typically actuated for large and medium-break LOCAs and also for some small-break scenarios. Containment spray systems have several purposes. The most immediate function is rapidly condensing the steam that would be released to the containment atmosphere to protect the structural integrity of the containment building from overpressurization. Spray systems also scavenge gaseous fission products such as radioactive iodine that might be released from damaged fuel elements and sequester these products in solution to minimize their long-term release to the environment. Finally, spray systems deliver and/or distribute chemical additives that prevent the pH of the containment pool from becoming acidic. Acidic environments greatly accelerate corrosion processes for many structural metals and reduce the solubility of iodine in solution. Reactor coolant water issuing from a broken pipe would

be slightly acidic from the addition of boric acid, which serves as a burnable neutron poison, and radiolysis of water would produce hydrogen ions that lower pH, so chemical additives are necessary to prevent long-term acidification of the recirculation pool.

Three basic chemical additive systems are presently in service across the nuclear utility industry: (1) injection of concentrated sodium-hydroxide solution with the spray water, (2) dissolution of dry trisodium phosphate stored in baskets on the containment floor, and (3) melting of ice columns containing concentrated sodium tetraborate. The phosphate system has a target pH of approximately 7.0 for a well-mixed pool, and the sodium systems have a target pH of between 9.0 and 10.5; however, local pH values can be much higher before the additives are thoroughly mixed in the entire recirculation volume. STP utilizes option 2, dissolution of dry trisodium phosphate.

Although pH control is designed to prevent chemical attack on structural materials, there is growing evidence of unintended detrimental effects of these chemicals with regard to recirculation-sump operability. First, it is well known that high-pH, high-temperature environments enhance the corrosion of aluminum. For this reason, nuclear power plants control their containment inventory of exposed aluminum surfaces and are designed to prevent a catastrophic deflagration of hydrogen gas that can accumulate as a byproduct of aluminum oxidation. It is also known that various species of aluminum hydroxide can form amorphous, gelatinous suspensions that could pose severe head-loss consequences if accumulated on a fibrous debris bed. Concerns over potential adverse chemical effects in the containment environment were initially substantiated by a somewhat qualitative description of gelatinous material recovered from the containment sump at Three Mile Island many months after the accident. The ICET test program confirmed the plausible formation of at least two reaction products that may exacerbate sump-screen head loss.

The dominant potential product formation mechanism at STP is postulated to be corrosion of submerged aluminum with subsequent formation of aluminum oxy-hydroxide. Two chemical forms pose possible concerns: (1) nucleation and crystalline growth directly on fiber-glass debris strands, and (2) precipitation of an amorphous compound in the bulk solution with subsequent migration to the debris bed.

As part of the GSI-191 research program, the ICET series investigated the potential for chemical interactions between the cooling water and exposed materials within the containment structure. To simulate these potential interactions, structural materials and solution compositions determined to coexist within a post-LOCA containment environment were placed into a 250-gal. stainless steel (SS) tank and allowed to interact for thirty days under constant observation. The proportion of sample materials exposed to the solution and suspended above the solution was properly scaled to the volume of water to preserve representative ratios of corrosion surface and dilution volume that may be present in PWR containment buildings. All five tests performed within the ICET series used the set of exposed sample materials itemized in Table 1-1. All five tests maintained a constant temperature of 60ºC±2ºC at atmospheric pressure with the same baseline reactor-coolant chemistry, but the simulated insulation debris and the pH control system varied as defined in Table 1-2.

CHLE tests focus on STP conditions similar to ICET #2 except that material inventories have been adjusted to be plant specific and temperature is now controlled to emulate a post-LOCA cooling history. CHLE uses the same 250-gal. tank that was constructed for ICET, but three additional flow circuits have been added to accommodate the introduction of replicate fiberglass debris mats. A heat exchanger is also included to emulate the temperature cycle experienced in the plant as water moves from the containment pool through residual heat removal (RHR) and through the hot reactor core (Ref. 44).

Figure 1-1. CHLE test apparatus showing chemical corrosion tank (left) and 3 parallel circulation columns (right). All components are wrapped in thermal insulation.

Table 1-1. Material-Quantity/Sump-Water-Volume Ratios for the ICET Tests

Material	Ratio (ratio units)
Zinc in Galvanized Steel	8.0 (ft^2/ft^3)
Inorganic Zinc Primer Coating (non–top coated)	4.6 (ft^2/ft^3)
Inorganic Zinc Primer Coating (top coated)	0.0 (ft^2/ft^3)
Aluminum	3.5 (ft^2/ft^3)
Copper (including Cu-Ni alloys)	6.0 (ft^2/ft^3)
Carbon Steel	0.15 (ft^2/ft^3)
Concrete (surface)	0.045 (ft^2/ft^3)
Concrete (particulate)	0.0014 (lbm/ft^3)
Insulation Material (fiberglass or calcium silicate)	0.137 (ft^3/ft^3)

Table 1-2. Experimental Conditions in the ICET Tests[1,2]

Test #	Boron[3] added (mg/L)	NaOH added (mg/L)	TSP[4] added (mg/L)	Test pH range	pH buffering agent[5]	Insulation Debris Volume[6]	
						Fiberglass	Calcium Silicate
1	2,800	7,677	-	9.3 – 9.5	borate	100%	-
2	2,800	-	4,000	7.1 – 7.4	phosphate	100%	-
3	2,800	-	4,000	7.3 – 8.1	phosphate	20%	80%
4	2,800	9,600	-	9.5 – 9.9	borate	20%	80%
5	2,400	-	-	8.2 – 8.5	borate	100%	-

Notes:

1. Temperature was maintained at 60°C ± 3°C in all tests.
2. The following chemicals were also added to the solution: LiOH = 0.7 mg/L and HCl = 100 mg/L in Tests #1 through #4. LiOH = 0.3 mg/L and HCl = 42.8 mg/L in Test #5. Also, 63.7 g of latent debris and 21.21 g of concrete dust were added to the mixture prior to each test initiation.
3. The required boron concentration of 2,800 mg/L was added as 16,000 mg/L H_3BO_3 in Tests #1 through #4. To attain the required boron concentration of 2,400 mg/L for Test #5, 18,500 mg/L of $Na_2B_4O_7 \cdot 10H_2O$ (sodium tetraborate) in 143 gal. of water was added to 16,000 mg/L of H_3BO_3 in 107 gal. of water.
4. Trisodium Phosphate (TSP) = $Na_3PO_4 \cdot 12H_2O$.
5. While other additives establish system pH on a wide scale, the buffering agent keeps pH relatively stable by resisting minor fluctuations from its pK_a.
6. All tests consisted of 0.137 cubic feet of insulation represented per cubic foot of water. For each test, the insulation was present as fiberglass and/or calcium silicate material with the proportion of volume shown in the table.

2 THEORY DEVELOPMENT

One recurring complication of testing fibrous debris beds that have been associated with ECCS sump blockage is an observed decrease in bed thickness under flowing conditions. For convenience and clarity of discussion, reduced bed thickness will be attributed to two basic mechanisms: (1) relatively rapid compression and (2) more gradual compaction. The term "compression" is used here to refer specifically to a change in bed thickness caused by mechanical transmission of forces between debris elements that are locked in a physical arrangement of linkage points. In the case of fiberglass, loads induced by hydraulic resistance can be supported by internal tensile properties of the fibers. When the load is released under pure compressive conditions, bed thickness is fully recovered in the manner of a spring returning to its uncompressed length.

"Compaction," by contrast, will be used to describe a collection of processes that lead to irrecoverable decreases in bed thickness. These processes include migration of particulates to achieve higher packing ratios, rotation of fiber flocks to fill internal voids, slippage of fiber contact points, breakage of fibers under excessive tensile stress, etc. Compaction always involves relative movement between debris elements and, in general, refers to mechanisms that relax or dissipate internal stresses caused by water flowing through the bed. A simple analogy of a possibly common compaction mechanism in fiberglass is provided by the following mental experiment. Stand a common paperclip on edge under the pressure of your finger and exercise the tensile spring by pushing hard enough to cause elastic deformation (flex). If the paperclip rotates or slips under nonequilibrium forces and lies flat, the opportunity for tensile recovery is lost and a significant thickness reduction has occurred. Compaction processes continue until the equilibrium static load imposed on a debris element under contact with its neighbors exceeds local drag forces available to induce motion. One final distinction is that compaction processes can continue reducing bed thickness after all tensile recovery potential has been dissipated.

One objective of the STP vertical head-loss study will be to compare, and to quantify where possible, the hydraulic resistance properties of various chemical products that may be identified in the CHLE test program. These products may either form directly on the fiberglass mat or they may precipitate from bulk solution and migrate to the debris bed. Bed-thickness reduction complicates the task of characterizing chemical head loss by amplifying in a positive feedback loop pressure losses that are initiated by the inherent resistance of the debris elements; initial compression and compaction leads to greater hydraulic resistance, and hence, to greater thickness reductions, etc. Thickness reduction is initially resisted by the inherent tensile properties of long fibers present in the bed, and it is ultimately limited by the solid density of the debris material. Thus, the physical configuration of the bed can evolve under continuous flow in a manner that is difficult to quantify, and these changes introduce uncertainties into any analysis of corresponding pressure-loss data.

Relationships between local debris-bed density and hydraulic resistance are developed in Section 2.1 to provide a means of expressing internally distributed hydraulic forces in terms of measurable variables like the bulk approach velocity and unknown properties of the debris like the specific surface area (material area divided by material volume). This detailed approach supports development of a coupled head-loss correlation that properly accounts for bed compression and compaction under flow. Rigorous derivations of hydraulic gradient may also help identify the degree of approximation inherent to standard head-loss correlations, even if the assumption of homogeneity is adopted later for practical reasons.

2.1 Flow Through Porous Media

Fundamental arguments based on momentum transfer and viscous shear are reviewed in this section to explain the origin of the classic porous medium head-loss equations developed by Davies and Ergun (Refs. 10 and 12). This careful treatment will help enumerate assumptions that have become implicit over many years of use and correct some misconceptions that have crept into the vernacular of porous media flow prediction. Several refinements to the standard methods are also explored that may warrant comparisons with experimental data for problematic debris types such as calcium silicate particulates, gelatinous chemical deposits, and stratified layers of paint chips.

Several definitions of area are used throughout this section. They are itemized here to provide both an advance warning and a convenient reference:

- A_A far-field approach area defined by the outer dimensions of the clean filter extending perpendicular to the flow direction,
- A_S geometric area of clean screen without consideration of open fraction,
- A_C circumferential area of a fully loaded convoluted strainer design,
- $A(z)$ interstitial flow area existing at any horizontal plane in a 1-D bed,
- A_M physical area of a mesh or perforated plate that obstructs flow,
- $S_V(z)$ local specific surface area of debris $\{m^2/m^3\} = \{m^{-1}\}$ defined as the debris surface area per unit of solid debris volume.

2.1.1 Derivation of Pressure Gradient Formulas

Practical concerns regarding debris blockage center around the total pressure difference occurring across opposing sides of the bed. However, the internal processes of compression and compaction are driven by internal distributions of hydraulic force, the computation of which requires an expression of the pressure gradient within the bed. Pressure gradient formulas are developed in this section based on classical descriptions of momentum flux, gravitational body force and boundary layer shear stress. Pressure gradient contributions from inertial drag are presented in Section 2.1.3.

2.1.1.1 Momentum Flux Within a Control Volume

The first section to follow introduces the geometry and bed-morphology assumptions that will be used throughout this development (Section 2.1.1.1.1). Proceeding sections introduce the momentum equation as a governing principle with a derivation of momentum efflux from a control volume (Section 2.1.1.1.2), offer an optional discussion of vertical-flow probability distributions to partially compensate for the limitations of a one-dimensional velocity distribution (Section 2.1.1.1.3), and describe the expansion of depth dependencies that will motivate spatial descriptions of debris-bed structure (Section 2.1.1.1.4).

2.1.1.1.1 Geometry and Background Assumptions

Figure 2-1a illustrates water approaching a composite debris bed with a flow velocity of $w_A = Q / A_A$ where Q is a constant volumetric flow rate and A_A is the total approach area. For prototypical flat sump screens, A_A is generally assumed to be equal to the total geometric area of the screen A_S without regard to the actual open area of the mesh or perforated plate. The geometric screen area is determined by the largest outer dimensions of the screen and is reduced to account for any flow area blocked by structural bracing. For complex convoluted screens that gradually fill with debris, the approach area can gradually transition from A_S to the outer circumscribed area of the entire three-dimensional strainer A_C; circumscribed area can depend on the thickness of the debris and on any preferential loading pattern that may occur. In combination with the volumetric flow rate, A_A sets the entrance velocity boundary condition by defining the face area presented by the bed to the flow.

The strainer exit velocity w_E is determined by the local interstitial flow area of the debris bed next to the strainer $A(L)$ minus the portion of area A obstructed by the screen that is *not* also covered by debris. Since A/A_S is the fraction of open area in the debris next to the screen, $A_M\left(A/A_S\right)$ is the additional flow area obstructed by a mesh of total area A_M. The exit velocity is then $w_E = (Q/A)(1 - A_M/A_S)^{-1}$ where the interstitial flow area A is evaluated at the bottom of the bed at $z = L$. In a typical test configuration where water passes vertically downward through a debris bed supported within a cylindrical pipe, mass conservation requires that the bulk water velocity quickly return to w_A.

Throughout this development it is assumed that the volumetric flow rate Q is constant. Each emergency-core-cooling-system (ECCS) recirculation pump is rated to provide at least a minimum required design flow when supplied with a minimum required net positive suction head ($NPSH_R$) at the centerline of the pump bore. This means that a minimum fluid pressure must exist at the entrance to the pump to ensure proper performance and to avoid complications like cavitation and air ingestion. The actual flow rate of a pump depends on its mechanical performance characteristics, which vary as a

function of both the inlet and the outlet pressure conditions. These conditions change during the course of a postulated accident sequence, so the exact flow rates will also change. The net positive suction head available ($NPSH_A$) to feed a pump can depend on many factors including the elevation difference between the floor of containment and the pump inlet; the depth of water in the containment pool; the length, complexity, and manufacture of supply piping from the sump to the recirculation pump; the overpressure

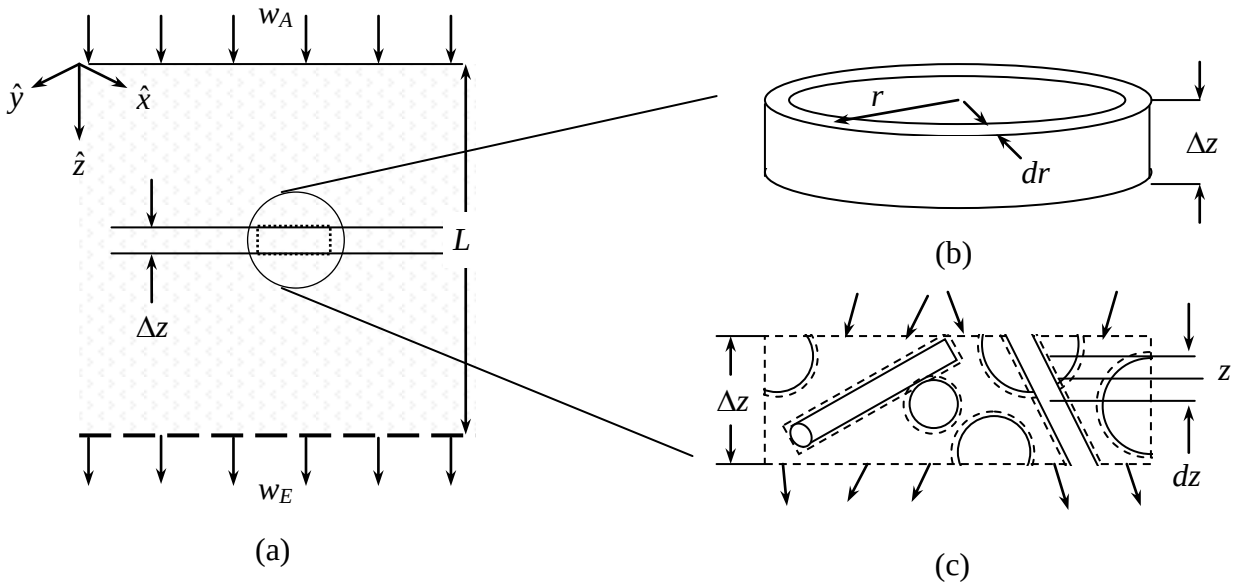

Figure 2-1. Geometry of flow through a one-dimensional porous medium: (a) bulk approach and exit velocities, (b) cylindrical differential volume element, (c) internal velocity vectors penetrating a control system of fluid (dashed boundary).

that exists in the containment building; and various attributes of the clean strainer design like its fabrication of mesh or perforated plate, whether or not the strainer is fully submerged in water, and its geometry within the recirculation pool. The difference between available suction head and required suction head is defined as the net positive suction head margin ($NPSH_M$), and the presence of debris on the sump screen can erode this margin to the point of pump failure. Thus, the actual flow rate that is pulled through a debris bed is coupled to the pressure drop experienced across the bed through the mechanical response of the pump. However, for the purpose of debris-bed head-loss prediction, it is sufficient to assume a constant instantaneous flow rate and to relegate feedback mechanisms to a system-wide vulnerability assessment.[1]

Consider now the microscopic characteristics of flow through a porous medium and, following the formalism presented in Ref (13), define a "system" of water passing through a differential annular volume of debris in a one-dimensional composite bed as

[1] The various components of net positive suction head have specific regulatory definitions delineated in Regulatory Guide 1.82 (Ref. 36) that may differ slightly from the operational descriptions discussed here.

shown in Figure 2-1b. The system of interest comprises the water within the debris volume at the instant in time that is illustrated. At this instant, the water occupies a control volume (CV) defined by the dashed boundary in Figure 2-1c. The system of water will continue to pass through the CV immediately thereafter, but the CV is stationary. Again, note that the CV includes only fluid in the interstitial space within the differential volume and not the debris material forming the porous medium. Debris obstructions represent surface areas where viscous shear dissipates energy and imparts drag forces on the CV. A debris bed can be treated as one dimensional if the composition, morphology, and internal velocity profiles vary only from top to bottom and not from side to side. This condition generally holds when the thickness of a contiguous bed is small compared to its lateral extent so that edge effects can be ignored, but obviously, there exists a spatial scale small enough that three-dimensional flow patterns around the debris elements become important.

It will also be required that debris elements have random orientations that create azimuthally isotropic internal velocity fields, at least on a scale greater than a few particle or fiber diameters. This condition implies that there is no preferred lateral flow direction. As the fluid penetrates through the medium, all possible side-to-side deflections are equally likely, and no net lateral forces are exerted on the bed as a whole that would induce motion if the bed were not restrained by a rigid outer structure. (Small-scale lateral force imbalance may continue to induce bed reconfiguration and particulate migration, however). For randomly oriented debris, it is generally understood that a one-dimensional bed will have an azimuthally isotropic velocity field regardless of what entry point is chosen as a reference. A careful treatment is only needed for regular arrays of flow obstacles such as vanes and lattices that are designed to divert flow in specific directions. Even relatively well-ordered layers of paint chips would not be expected to introduce preferred lateral directions to the flow.

2.1.1.1.2 Derivation of Internal Forces

The sum of all directed body and surface forces acting on the fluid system shown in Figure 2-1 equals the net force imparted by changes in linear momentum $\vec{p}$ as defined by Newton's Second Law such that

$$\sum \vec{F} = \vec{F}_{Body} + \vec{F}_{Surface} = \vec{F}_{Momentum} = \left.\frac{d\vec{p}}{dt}\right)_{System} . \quad (1)$$

Because the moving fluid system and the stationary CV are coincident at the instant illustrated in the figure, the resultant forces acting on the system are the same as those acting on the CV.

The general relationship between changes of momentum in the system and changes of momentum within the control volume is given by

$$d\vec{p}/dt\big)_{System} = \frac{\partial}{\partial t}\int_{CV}\vec{V}\rho\, d\forall + \int_{CS}\vec{V}\rho\vec{V}\cdot d\hat{A} \tag{2}$$

where $\vec{V} = V\left(\vec{r},\hat{\Omega}\right)$ represents the interstitial fluid velocity vector carrying a magnitude V at spatial position $\vec{r}$ in the angular direction $\hat{\Omega}$ [1]. The incompressible water density ρ depends on temperature but is assumed to be constant throughout the bed, and the first and second terms of the above relation represent integrals over the entire control volume (CV) and control surface (CS) of that volume, respectively. Again, A represents the interstitial flow area at the faces of the CV, which has differential elements $d\hat{A}$ directed outward along local, surface-normal, unit vectors. For the moment, A implicitly represents the local porosity of a bed at any depth z, but the porosity can be introduced explicitly as a ratio of the interstitial area to the geometric approach area at the same depth, i.e., porosity $\varepsilon(z) = A(z)/A_A(z)$. Generally, the flow path circumscribing the bed will have a constant cross section so that $A_A(z) = A_A$.

Equations (1) and (2) can be equated to yield the momentum-force equation for an arbitrary CV. Under steady-state flow conditions there are no time variations of velocity within the bed, so the simplified result is

$$\vec{F}_{Momentum} = \vec{F}_{Body} + \vec{F}_{Surface} = \int_{CS}\vec{V}\rho\vec{V}\cdot d\hat{A}. \tag{3}$$

Equation (3) states that the sum of all forces acting on a CV is equal to the net rate of linear momentum efflux. The associated surface integral will be referred to as the momentum force $\vec{F}_{Momentum}$ throughout this section. In an azimuthally isotropic velocity field, fluid exiting the sides of the annular volume shown in Figure 2-1b will be balanced by fluid entering those faces. Thus, there will be no net momentum exchange from the sides and only one equation of motion is needed to describe fluid flow along the z direction. No fluid will cross the internal boundaries of the control surface where flow must be tangent to the surface of the debris elements, so only the top and bottom of the annular volume need to be treated rigorously in order to evaluate the surface integral.

While bulk flow moves through a debris bed in a predominantly vertical direction, obstacles divert water and impart lateral velocity components to the field. In return, these local perturbations in momentum exert hydraulic forces on the debris elements. Along any streamline crossing the upper or lower boundary of the annular CV, $\vec{V}\cdot d\hat{A} = \left|\vec{V}\right|\left|d\hat{A}\right|\cos\alpha$ where α is the angle between the outward surface normal and the local velocity vector. (Note that $\left|d\hat{A}\right| = 1$ by definition). It is reasonable to assume that the velocity magnitude and the diversion angle are related by location relative to the debris surface, so the two cannot be decoupled without introducing some approximation.

[1] A fluid velocity field takes a single discrete direction at each spatial location, unlike a radiation field which is generally distributed in all directions, all energies, *and* distributed in the volume about each spatial point.

However, they will be treated as independent factors in this development. Flow diversion induces a distribution of α within the available flow area that is peaked near π on the entrance face and peaked near 0 on the exit face; and, one might expect that the volume-averaged magnitude of lateral velocity components will increase with decreasing porosity ε. Regardless of deflections in the fluid velocity, lateral homogeneity and mass continuity require that the volumetric flow rate, when suitably averaged over local perturbations, must be constant at every depth in the bed. Thus, the velocity field must accelerate or decelerate to accommodate the constraint that $\int \vec{V} \cdot \hat{k}\, dA = Q$ for surface integration over any horizontal plane intersecting the bed at arbitrary depth z. The unit vector $\hat{k}$ defines the positive direction of the z coordinate.

The scalar product of velocity and directed surface area in Eq. (3) defines the volumetric flow rate across the surface element, the factor ρ converts the product to mass flow rate, and the additional factor of $\vec{V}$ converts the product to force and reassigns the flow direction to ensure appropriate vector summation through the process of integration. If the velocity field is azimuthally isotropic over a spatial scale comparable in size to several adjacent debris elements, then there is no net momentum transfer perpendicular to the bulk flow and Eq. (3) can be reduced to a summation of vertical force components only. It follows that $\int_{CS} \vec{V} \rho \vec{V} \cdot d\hat{A} = \rho \int_{CS} \left(\vec{V} \cdot \hat{k} \right) \left(\vec{V} \cdot d\hat{A} \right) \hat{k}$.

Comparison of the four cases for flow vectors entering and exiting the top and bottom surfaces of the CV shows that the two factors in the above integral have the same sign for the bottom surface ($d\hat{A}$ and $\hat{k}$ coincident) and opposite sign for the top surface ($d\hat{A}$ and $\hat{k}$ opposed). Thus, the assumption of azimuthal symmetry for a one-dimensional bed, which also must hold at every depth z, can be enforced by expressing Eq. (3) as

$$F_{Momentum} = \rho \left[\int_{bot} V^2 \cos^2\theta \, dA - \int_{top} V^2 \cos^2\theta \, dA \right] \tag{4}$$

where θ is the angle between the velocity vector and the positive z coordinate (i.e., the polar direction angle) and the equation is understood to describe vertical force components only. Because the signs of each term are now explicit, orientation of the differential surface elements is no longer required. For continuous bulk flow through a bed it should be expected that $0 \le \theta \le \pi/2$, which simply means there is no reverse flow.

Possible effects of lateral flow diversion on momentum changes in the fluid are traditionally neglected from Eq. (4) based on arguments that (1) fibrous beds are very porous $(\varepsilon > 90\%)$ so the spatially averaged deflection angle at any horizontal cross section will be small, (2) the cosine is insensitive to small changes in the argument near 0 and π, (3) primary interest is usually focused on the total pressure difference across a debris bed between pressure transducers placed in a constant-volumetric-flow system where the upstream and downstream velocity fields are designed to be identical so that

net $F_{Momentum} = 0$, and (4) high-resolution velocity information needed to carefully quantify interstitial fluid-momentum variations is not usually available. For highly compact particulate beds, potentially deformable gelatinous deposits, and regular orientations of paint chips this approximation may not be appropriate. As an extreme illustration of the possible effects of debris morphology, consider that a bed of platelets aligned perpendicular to the bulk flow direction will impart a much greater deflection than the same platelets aligned parallel to the flow even if the two configurations have the same bulk porosity.

2.1.1.1.3 Vertical Flow Probability Distributions

Fine details in the interstitial velocity field are needed to determine the degree of lateral flow deflection present at any point within the bed. In this section is presented a strategy for parameterizing these details into a single geometry coefficient, β. However, high-resolution velocity fields are seldom available for engineering applications, so the full explanation of the statistical averaging process can be omitted without loss of continuity. It will be sufficient for most readers to understand that β represents a correction factor that accounts for the presence of nonvertical velocity components and to continue with Section 2.1.1.1.4. The traditional treatment of the momentum force surface integral can always be recovered by setting $\beta = 1$.

One means of alleviating the apparent contradiction between the simplification of lateral homogeneity needed for one-dimensional bed behavior and the physical occurrence of local velocity perturbations around debris elements is to collapse all angular velocities observed within a finite thickness centered on a horizontal plane into a joint probability distribution defined on the ranges of both velocity magnitude and lateral deflection angle that preserves the spatially averaged behavior of the field. The thickness Δz of spatial averaging required to define this distribution should not exceed the size of several adjacent debris elements as suggested in Figure 2-1c. As a practical consideration, lateral homogeneity of the bed limits the required lateral range similarly so that the distribution of angular velocity can be compiled over any unit cell of representative spatial complexity. The size of the required representative cell may vary depending on the bed composition and morphology.

Of course, computation of a velocity probability distribution would require complete knowledge of the velocity-vector field $V\left(\vec{r}, \hat{\Omega}\right)$ defined at all spatial locations $\vec{r}$ and angular directions $\hat{\Omega}$ within a debris bed having a very specific configuration. This complication will be accepted for the moment in favor of the notational convenience and the generality offered by the concept of a probability distribution for investigating the effects of debris-bed morphology on internally distributed hydraulic forces. The formalism may also help to suggest convenient scaling rules and appropriate parameterizations for the application of empirical data. It is possible that computational fluid dynamics (CFD) models may be applied to obtain velocity fields for idealized and prototypical debris configurations, or alternatively, that analytic solutions for external

flow over regularly shaped objects may be superimposed to approximate the internal velocity field. Even generic exercises of this nature may help to quantify the possible magnitude of momentum transfer that is imposed on the angular velocity distribution by a specific debris combination.

Here, bed morphology will be denoted by the state vector $\vec{\xi}$, which includes such attributes of the debris elements as local spacing (porosity), size distributions, aspect ratios, spatial arrangement, surface complexity, etc. To illustrate the diversity of possible debris configurations, compare the features of (1) a sand bed composed of random, semispherical, discrete grains; (2) a bed of paint chips composed of regular, stratified layers of platelets; (3) a bed of loosely compacted fibers whose elements have extremely large aspect ratios, infrequent points of contact, and significant tensile properties; and (4) gelatinous chemical deposits within a fiber network that may deform, vibrate, or agglomerate under flow. In traditional treatments of flow through porous media, the effects that these differences introduce to hydraulic losses are often captured by applying empirical correction factors to basic formulas that were derived under simplified flow conditions. In this development, theoretical correction factors will be introduced explicitly to help direct the most effective application of empirical evidence

To render more tractable the problem of defining a probability function that describes the spatially averaged distribution of velocity magnitude and deflection angle, consider only variations in the vertical velocity component $w = V\cos\theta$ across an arbitrary horizontal slice of the debris bed. Any inherent dependence between speed and direction has now been combined into a single metric related to volumetric flux. (In some cases, it might be determined that this metric alone is adequate to describe the unique characteristics of a given debris bed). The vertical velocity component is a simple scalar field that can be generically illustrated as a function of location on the plane as shown in Figure 2-2. Now, the task of defining a probability distribution for the flow field reduces to a procedure for answering the question, what portion of interstitial area on the plane is crossed by fluid having a vertical velocity component w? The exercise of computing relative areas each associated with a range of velocities will permit the collapse of two-dimensional flow variations onto a single spatial point that represents the angular complexity of the one-dimensional velocity field.

Stated more formally, the present objective is to find a function $g(w)$ that is distributed per unit velocity such that $g(w)\,dw$ is the probability of a streamline crossing the plane in the vertical velocity range dw about w. All fluid crossing the plane must have a finite vertical velocity, so as expected for a probability distribution, the following normalization must hold $\int_0^\infty g(w)\,dw = 1$. Figure 2-2 suggests that the probability of crossing the plane with a given velocity w can be approximated numerically by

computing the contour area that lies between two values of the velocity field and dividing by the total interstitial area across the plane. For the example shown, $P(w) \approx \Delta A / A \approx g(w)\,\Delta w$, so the desired probability density is approximated as $g(w) \approx \Delta A / (A\,\Delta w)$.

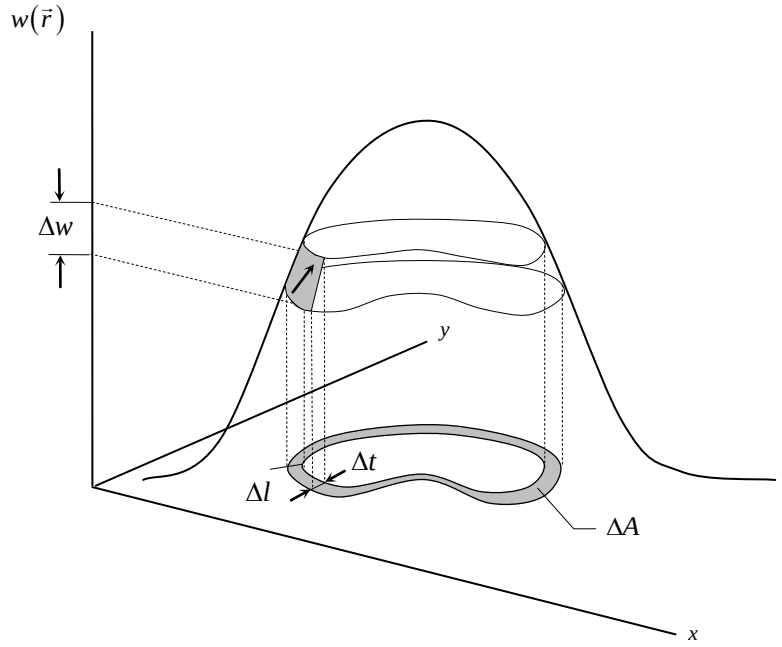

Figure 2-2. Schematic function of the vertical velocity component that might exist across any horizontal plane intersecting the debris bed.

The increments labeled in Figure 2-2 can also be interpreted as differential intervals, which suggests a continuum definition for the probability distribution. Consider a facet of area on the scalar velocity function as shown in Figure 2-2. The magnitude of the local gradient $\vec{\nabla} w = \frac{\partial w}{\partial x}\hat{i} + \frac{\partial w}{\partial y}\hat{j}$ provides the relationship between a differential interval of velocity and the distance between two contours projected in the plane, i.e. the slope (rise/run) such that $\left|\vec{\nabla} w\right| = dw/dt$ where t is the planar length of the projected gradient direction. The facet has a projected area of $dt\,dl$ that can be integrated around the contour to yield the differential area centered about the contour $dA = \oint dt\,dl$ where the circle denotes a closed integration path. By analogy with the discrete approximation given above and substitution of dt through the definition of the slope, an expression for the desired probability function can be found, $g(w) = A^{-1} \oint \left|\vec{\nabla} w\right|^{-1} dl$. Thus, the value of the probability function for a given velocity can be computed by integrating the reciprocal of the velocity gradient magnitude around the locus of points associated with

all contours of the desired velocity and normalizing by the interstitial open area. The probability function can be evaluated in this manner for a number of discrete velocities and then numerically integrated and renormalized to smooth the approximation.

The probability distribution of the vertical fluid velocity components that exist across the plane provides a weighting function that can be used to compute the area-weighted average vertical velocity. As with any properly normalized statistical distribution, the mean is given by the first-moment integral, so $\bar{w} = \int w g(w)\, dw$. The average vertical velocity can also be computed from the constant volumetric flow rate and the interstitial area across the plane as $\bar{w} = Q/A$, so the volumetric flow rate must be proportional to the first moment of the velocity distribution $Q = A\int w g(w)\, dw$. It is also true that the volumetric flow rate is defined by the spatial integral of the vertical velocity function $Q = \int w(\vec{r})\, dA$, so a useful mapping has been found between two-dimensional integration over the spatial velocity field and integration over the velocity probability distribution. Because both expressions for volumetric flow rate imply full integration over respective domains, it must be true that

$$w(\vec{r})\, dA = A w g(w)\, dw. \tag{5}$$

Now that a connection has been established between the spatial location and the velocity probability distribution as indices of vertical velocity magnitude, the force of momentum transfer acting on the CV can be written as

$$F_{Momentum} = \rho\left[\int_{bot} A w^2 g(w)\, dw - \int_{top} A w^2 g(w)\, dw\right] \tag{6}$$

by substitution of Eq. (5) in Eq. (4). Now, it is apparent that the force exerted on a fluid moving across a boundary is proportional to the second-moment integral of the velocity probability distribution. This is a result commonly obtained in the development of integral forms of the momentum equation for a CV (Ref. 41). Note that the interstitial area has not been treated as a common factor because it may vary with location in the bed. Derivations that treat directly the areal integral of Eq. (4) usually neglect the fact that the integration limit can be a function of depth in the bed.

A more familiar form of Eq. (6) can be obtained by factoring the local area-averaged velocity from the integrals. This is accomplished by substituting a scaled dimensionless velocity defined as $\tilde{w} = w/\bar{w}$. Because the probability density function $g(w)$ is distributed in velocity, a new dimensionless function must be defined that preserves the relationship $g(w)\, dw = h(\tilde{w})\, d\tilde{w}$, but the velocity is not a distribution function so it can be replaced by direct substitution. The generic result obtained after these changes for the force exerted on any horizontal plane of fluid is $F = \rho A \bar{w}^2 \int \tilde{w}^2 h(\tilde{w})\, d\tilde{w}$. Given the

probability density $g(w)$ for vertical velocity, the dimensionless distribution $h(\tilde{w})$ can be computed as $h(\tilde{w}) = g(w)(dw/d\tilde{w}) = \bar{w}g(w)$.

With the substitutions defined above, Eq. (6) can be written as

$$F_{Momentum} = \rho\left[A\bar{w}^2\beta\Big|_{bot} - A\bar{w}^2\beta\Big|_{top} \right] \tag{7}$$

where $\beta\left(z,\vec{\xi}\right) = \int \tilde{w}^2 h(\tilde{w})d\tilde{w}$. Recall that all factors except density depend on location within the bed, and note that $\beta = 1$ for conditions of unperturbed uniform flow where $\tilde{w}^2 = 1$ and $\int h(\tilde{w})d\tilde{w} = 1$. Knowing that $\int_0^\infty h(\tilde{w})d\tilde{w} = 1$, β can be interpreted as the positive, probability-weighted square of dimensionless vertical velocity. It is possible to imagine distributions of vertical velocity $g(w)$ that are skewed either above or below the mean velocity $\bar{w}$, so β can have values either greater than or less than 1, respectively.

All features of momentum transfer within a porous medium that are related to bed morphology have now been captured in the dimensionless integral β. This factor will be referred to as the "bed-geometry factor." Classical developments either neglect this term and implicitly set $\beta = 1$ or invoke ad hoc geometric correction factors to achieve better agreement with empirical data. Here, peculiarities of fluid flow through a given debris type that impart distributed forces to the bed can be traced back to details of the interstitial velocity field. When stated explicitly in this manner, it is more difficult to assume complacently that β equals unity at all depths in every debris bed. Regardless of whether the distribution $h(\tilde{w})$ is computed numerically, investigated through microphysical experiments, or investigated parametrically, one important benefit of the formalism may be to focus attention on the possible separability of porosity and shape factor that are subsumed in the factor β. If, for example, it can be shown to a reasonable approximation that $\beta = a\left(\vec{\xi}\right)b(\varepsilon)$ where $a\left(\vec{\xi}\right)$ is a constant characteristic of the debris elements and $b(\varepsilon)$ represents spatial scaling by the local porosity, many analytic methods for superposition of composite debris types can be invoked.

A simple thought experiment that illustrates the dependence of β on porosity is to imagine a highly regular debris bed consisting of hard spheres of identical radii arranged in a body centered cubic configuration with a known packing factor (solidity) of 0.68 and a complementary porosity of 0.32. A formal value of β could be calculated by performing a volume-weighted average of vertical velocity computed by CFD throughout the unit cell. Now, inflate the unit cell in all directions without changing the particle size until the porosity is doubled to 0.64. The amount of lateral flow deflection per unit volume decreases and β will shift closer to the value of 1.0. Thus, there is a direct correlation between porosity ε and geometry factor β, but the neither the shape, size, or

relative configuration of the debris elements have changed. To express this dependence explicitly, let $\beta = \varepsilon^{\alpha}\zeta$ where ζ is the tortuosity and α is an empirical scaling parameter placed on the porosity. Other direct correlations with porosity may also be suitable.

From the perspective of hydraulic flow, a complete description of a debris bed requires the spatial definition of three independent attributes: the porosity ε, the tortuosity ζ, and the specific surface area S_V. Specific surface area defines the shape, including aspect ratio and basic geometry, and the surface complexity of a notional isolated debris element. Porosity defines the proximity of the debris elements within the packed bed. Tortuosity defines configurational morphology including orientation of the elements and their relative positions. All three attributes depend on the mixed composition of a debris bed and all three can vary as a function of depth within the 1-D strata. However, local values of each attribute are sensitive to different factors. Specific surface area is an innate property of the local debris composition that will not change unless the debris are deformable under hydraulic drag or under compressive load. Porosity can change through both compression and compaction mechanisms that pack more debris mass per unit volume. Tortuosity can only be changed by compaction that permits relative motion like migration and rotation. Bed compression, by contrast, does not change the orientation of the elements with respect to the flow or their orientation with respect to each other.

2.1.1.1.4 Expansion of Depth Dependencies

Returning now to Figure 2-1 and to Eq. (7), the spatial dependencies of interstitial area A, laterally averaged vertical velocity $\overline{w}$, and bed geometry β can be expanded about the midplane of a differential annular volume located at depth z using the incremental form of Taylor's series $f(x+h) = f(x) + hf'(x) + \ldots$ where $h = \pm dz/2$ and f' denotes the first spatial derivative of the desired function. Substituting this generic expression for each of the three factors, neglecting products of differentials in the multiplicative expansion, and simplifying leads to the relationship

$$F_{Momentum} = \rho\left(\frac{d}{dz}A\beta\overline{w}^2\right)dz = \rho\left[2(A\beta)\overline{w}\frac{d\overline{w}}{dz} + \overline{w}^2\frac{d}{dz}A\beta\right]dz\,. \tag{8}$$

On a bed-averaged basis, mass conservation requires that the constant volumetric flow rate $Q = A(z)\overline{w}(z)$ at any depth, so this result can be further simplified to obtain

$$F_{Momentum} = \rho A\left(\overline{w}\frac{d}{dz}\overline{w}\beta\right)dz\,. \tag{9}$$

Two features of Eq. (9) are worthy of mention. First, recall that $F_{Momentum}$ describes the net force imparted on a differential CV of fluid by changes in momentum incurred

between the top and bottom faces. This term of the force balance indicates that the result of momentum change will be manifest as a change in average vertical velocity, i.e. as a fluid acceleration, that is induced largely by changes in the local flow path attributes of porosity, tortuosity, and specific surface area. Second, substitution of the bulk volumetric flow rate Q introduces an implicit average over the entire face of the bed because local variations will cause nonuniformities in actual volumetric flow through any given differential area. Later, in the development of interstitial shear force, a similar expression for momentum transfer is written for a constant-cross-section cylindrical conduit, and it is more appropriate to use the form of Eq. (8) with the assumption that $\partial/\partial z\left(A\beta\right)=0$ in a constant cross section capillary because the differential mass flow rate across any given sector of the flow path is not required to be constant.

All elements of Eq. (9) except the fluid density depend implicitly on the geometry of the bed, and later in this treatise $\bar{w}$ will be expressed in terms of the constant volumetric flow rate Q so that local porosity becomes the fundamental parameter of interest. However, the present form facilitates direct comparisons with other approaches found in the literature. For example, if the geometry factor is assumed to be unity, the force imparted by net momentum change is found to be proportional to the factor $\rho\bar{w}\left(d\bar{w}/dz\right)$. This result emphasizes the physical constraint that there can be no net momentum change in the fluid if there is no velocity gradient through the bed, regardless of the flow magnitude. When the debris has spatially uniform properties, the internal velocity gradient $d\bar{w}/dz$ will equal zero except at the entry and exit boundaries of the bed; and if the acceleration upon entry is equal in magnitude to the deceleration upon exit, there will be zero net momentum change across a homogeneous bed.

Zero momentum change in the presence of a uniform velocity field should not be interpreted as the absence of inertial drag. The effect being examined presently is the local acceleration of fluid caused largely by changes in the porosity of the medium. Both acceleration and drag can be manifest as a change in the local fluid pressure, so they both must be considered in an accurate description of the internal pressure distribution. However, in typical experimental conditions where a fluid passes through the debris mat and returns to its previous velocity in a constant-cross-section conduit, any pressure changes caused by local acceleration and deceleration are assumed to be adequately represented by the analysis of viscous-shear, which is covered in Section 2.1.1.3.2, and the net fluid-momentum change across the bed is assigned to be zero. Inertial drag, to be discussed in Section 2.1.3.2, introduces a dependence of pressure-drop on the square of the approach velocity, and it is not uncommon to see this effect confused with the net momentum force given by Eq. (9), as will be illustrated in a following example.

The sign of the term $\rho\bar{w}\left(d\bar{w}/dz\right)$ in Eq. (9) is consistent with the directionality of forces required to produce the observed changes in fluid velocity considering that bulk flow must accelerate when entering the bed and decelerate when exiting because of corresponding decreases and increases in the flow area. These changes in velocity result from forces acting on the top and bottom CS of the fluid. If the average interstitial

vertical velocity is large compared to the approach velocity, then momentum forces corresponding to the positive gradient near the entrance may dominate any momentum effects that are distributed throughout the bed by microscopic accelerations. The same observation holds for the opposing momentum forces that are expressed in the negative velocity gradient occurring near the exit where the fluid returns to the initial bulk flow speed. This discussion emphasizes the importance of including velocity transition zones as boundary conditions when computing hydraulic forces on a debris bed, because forces acting on the fluid CV are transmitted to debris elements through the process of viscous shear, which depends on local velocity gradients.

A heuristic derivation of the momentum force given by Sinceros and Sinceros (Ref. 34, pp. 337 – 338) illustrates how a quadratic-velocity term can be rationalized by spatial averaging of velocity through the thickness of the bed. Using the present nomenclature, they write the momentum term for downward flow through an element of a porous medium having differential volume $d\forall$ as $F = ma = \rho\varepsilon d\forall\left(d\bar{w}/dt\right)$. Substituting $\varepsilon d\forall = Adz$ and $d\bar{w}/dt = \left(\partial\bar{w}/\partial z\right)\left(\partial z/\partial t\right) = \bar{w}\left(\partial\bar{w}/\partial z\right)$, they obtain $F = \rho A\bar{w}\left(\partial\bar{w}/\partial z\right)dz$. This result is identical to Eq. (9) presuming that $\beta = 1$. They next introduce a thickness-averaged interstitial velocity computed as $\bar{\bar{w}} = L^{-1}\int_0^L \bar{w}\left(z\right)dz$ (here, the double overbar denotes averaging over a second spatial dimension) and substitute a dimensionless velocity profile defined as $\bar{w}^*\left(z\right) = \bar{w}\left(z\right)/\bar{\bar{w}}$ such that $\partial\bar{w} = \bar{\bar{w}}\partial\bar{w}^*$. After these substitutions, the momentum force becomes $F = \rho A\bar{\bar{w}}^2\left[\bar{w}^*\left(\partial\bar{w}^*/\partial z\right)\right]dz$.

Now, the dependence of momentum forces on the square of the constant, bed-averaged velocity has been expressed explicitly and all spatial variations are relegated to the dimensionless velocity profile $\bar{w}^*$. Upon integration over the entire bed thickness under the assumption of uniform porosity, the authors claim that these spatial variations yield nothing more than a dimensionless numeric coefficient. Thus, the total inertial force acting on water in the bed can be written as $F = K_i\rho A\bar{\bar{w}}^2$ where K_i denotes an inertial force constant. In fact, the dimensionless velocity $\bar{w}^*$ will hold identical values at any two points located above and below the bed so that the spatial integral is zero. These arguments have not avoided the inherent dependence of momentum variations on the spatial gradient of velocity, and appear to provide only a rationalization of inertial drag based on the faulty premise that it arises from the net change in momentum. It is shown later in Section 2.1.3 that inertial drag depends on the local change in momentum caused by diverting flow around obstructions in the bed, and that the effect of drag is cumulative.

The previous exercise is instructive because it illustrates several attributes of porous flow equations that are developed using the same rationale as Sinceros.

- First, because the momentum term has been averaged over the entire bed thickness, derivations of all other force components must also be averaged over the entire bed. This means that estimates of incremental head loss ΔH should be applied to the entire bed thickness and not to discrete layers within

the bed unless special care is taken to treat the inertial force constant as a function of depth in correspondence with properly averaged local velocities. One goal of the present development is to explicitly preserve depth dependencies of all the force components and to identify their contributions to the total internal pressure gradient.

- Second, the dependence of K_i on the thickness of the bed suggests that head-loss data from beds with similar composition but differing depths should be correlated in terms of head loss per unit thickness $\Delta H/\Delta L$ to remove the confounding effects of total bed thickness. However, this recommendation may not apply well to highly compressible media where internal hydraulic loads are distributed across the complete mechanical system; under these conditions, bed averaging may not be appropriate at all.
- Third, the derivation of a quadratic-velocity term, which will be fully developed in Section 2.1.3.2, does not impose any conditions on the flow regime. Although it is common to hear practitioners of debris-bed analysis refer to the quadratic term as the "turbulent" component of head-loss, the distributed momentum forces derived here are not contingent in any way on the presence of turbulence. The momentum term may be larger for higher velocity flows where turbulent conditions are more likely to exist, but this relationship is coincidental. Ahmed and Sunada (Ref. 2) provide some useful guidance for introducing into the analysis a turbulence decomposition of the total vertical flow.
- Fourth, the approximation of Sinceros was not intended to capture spatial variations throughout the bed, and thus, did not consider carefully a spatial gradient of porosity or interstitial flow area.
- Finally, the exercise has illustrated the application of spatial averaging throughout the thickness of the bed as a technique to smooth over subscale physical details that were not relevant to the derivation under consideration at the time. Exactly the same method was adopted by Ahmed and Sunada, a reference sometimes cited as providing theoretical "proof" that debris-bed head loss must contain a term that is proportional to the square of velocity.

Given the present objective to develop a model of distributed hydraulic loads within a debris bed, it is more rigorous to retain the spatial dependence of velocity, interstitial area and bed complexity that is expressed in Eqs. (8) and (9). Simplifications and approximations can be applied at a later time as needed to best interpret available data.

2.1.1.2 Body Forces Acting on the Fluid

The only body force acting on the fluid contained within the differential CV shown in Figure 2-1 is gravity acting downward in the positive z direction. The mass of fluid in the CV is $\rho\varepsilon(z)d\forall = \rho A_A\varepsilon(z)dz = \rho A(z)dz$, so the body force needed for substitution in Eq. (3) is

$$F_{Body} = \rho g A dz . \tag{10}$$

2.1.1.3 Surface Forces Acting on the Fluid

Surface forces acting on the differential CV shown in Figure 2-1 include both the net pressure exerted across the top and bottom faces of the volume and frictional forces that exist within the fluid wherever there are velocity gradients caused by water contact with debris elements on the boundary of the CV. Frictional forces arise from two primary mechanisms: (a) viscous shear where the fluid dissipates energy internally through molecular friction and (b) inertial drag where momentum is transferred to the debris through direct impingement along a complex CS. At a molecular level, both of these phenomena depend on the fine geometric structure of the debris and on the velocity field that arises from fluid interactions with the surface. Both occur to some degree along any fluid/solid interface, and because the two share the same origins in molecular kinetics, they cannot be separated at a fundamental level. Despite their commonality, it is traditional to treat viscous shear and inertial drag as separate, additive force components that each has unique characteristics in the velocity regimes over which they dominate. Thus, the surface forces needed for substitution in Eq. (1) or Eq. (3) are usually expressed as

$$\vec{F}_{Surface} = \vec{F}_{Pressure} + \vec{F}_{Shear} + \vec{F}_{Drag} . \tag{11}$$

Formal expressions for the pressure forces and shear forces acting on the CV are developed in the next two sections, respectively. Inertial drag is discussed later in Section 2.1.3.2.

2.1.1.3.1 Pressure Forces Acting on CV Surfaces

In general, the force imparted by total hydraulic pressure P across a surface of area A is $F_{Pressure} = PA$ acting in a direction opposite of the surface normal; i.e. "on" or "against" the surface. No net forces exist across the sides of the CV shown in Figure 2-1 for a one-dimensional debris bed, so only the influx and efflux faces of the differential volume need to be considered in detail. Net vertical forces (defined in the direction of $+z$) caused by hydraulic pressure on the top and bottom surfaces are thus expressed as $F_{Pressure} = PA\big|_{top} - PA\big|_{bot}$. Expanding both the fluid pressure and the cross sectional flow path area by Taylor's series about an arbitrary depth z gives the following expression $F_{Pressure} = \left[P(z) - \frac{dP}{dz}\frac{dz}{2} \right]\left[A(z) - \frac{dA}{dz}\frac{dz}{2} \right] - \left[P(z) + \frac{dP}{dz}\frac{dz}{2} \right]\left[A(z) + \frac{dA}{dz}\frac{dz}{2} \right]$, which can be simplified by multiplicative expansion and omission of products between differentials to obtain

$$F_{Pressure} = -\left(\frac{d}{dz} PA \right) dz . \tag{12}$$

where both $P = P(z)$ and $A = A(z)$. As expected the force of pressure acting on the differential volume acts in the direction opposite of the pressure gradient. Also, note that P is a face-averaged quantity that is presumed constant across the bed at a given depth. Minor variations caused by local acceleration in the fluid velocity have been subsumed in the average.

It will be convenient to expand the derivative across the product of local pressure and flow area to obtain the form

$$F_{Pressure} = -P\frac{dA}{dz}dz - A\frac{dP}{dz}dz, \tag{13}$$

which exposes the total pressure gradient for a decomposition into additive components,

$$\left(\frac{dP}{dz}\right)_{Total} = \left(\frac{dP}{dz}\right)_{Shear} + \left(\frac{dP}{dz}\right)_{Drag} + \left(\frac{dP}{dz}\right)_{Other}. \tag{14}$$

The first term on the RHS of Eq. (13) will be tracked as a component of $(dP/dz)_{Other}$ as will the body force and part of the momentum force. Contributions to the pressure gradient from these terms will be considered in Section 2.1.4. The linear decomposition of total pressure gradient is constructed for convenience to match the force decomposition given in Eq. (11). Even though the underlying phenomena are not fully separable, independent treatments of shear and drag are generally added to approximate the total pressure gradient.

Combining Eq. (3), and Eq. (11) yields a format of the force balance that emphasizes ultimate interest in the total pressure gradient

$$\vec{F}_{Pressure} = \vec{F}_{Momentum} - \vec{F}_{Body} - \vec{F}_{Shear} - \vec{F}_{Drag}.$$

Substituting previous expressions from Eq. (13), Eq. (8), and Eq. (10) leads to

$$\left[-P\frac{dA}{dz} - A\frac{dP}{dz}\right]dz = \left[2\rho(A\beta)\bar{w}\frac{d\bar{w}}{dz} + \rho\bar{w}^2\frac{d}{dz}A\beta\right]dz - \rho gAdz - \vec{F}_{Shear} - \vec{F}_{Drag}$$

$$-\left(\frac{dP}{dz}\right)_{Total} = \left[2\frac{\rho}{A}(A\beta)\bar{w}\frac{d\bar{w}}{dz} - \frac{1}{A}d\vec{F}_{Shear}\right] - \frac{1}{A}d\vec{F}_{Drag} + \left[\frac{P}{A}\frac{dA}{dz} + \frac{\rho}{A}\bar{w}^2\frac{d}{dz}A\beta - \rho g\right]. \tag{15}$$

Equating respective terms of Eqs (14) and (15) establishes three relationships that must be solved to evaluate the total pressure gradient through an inhomogeneous debris bed

$$-\left(\frac{dP}{dz}\right)_{Shear} = 2\frac{\rho\beta}{A}A\overline{w}\frac{d\overline{w}}{dz} - \frac{1}{A}d\vec{F}_{Shear}, \quad \text{(a)}$$

$$-\left(\frac{dP}{dz}\right)_{Drag} = -\frac{1}{A}d\vec{F}_{Drag}, \quad \text{(b)} \qquad (16)$$

$$-\left(\frac{dP}{dz}\right)_{Other} = \frac{P}{A}\frac{dA}{dz} + \frac{\rho}{A}\overline{w}^2\frac{d}{dz}A\beta - \rho g. \quad \text{(c)}$$

The pressure change in the direction of flow through complex debris is negative in almost all practical applications, so the explicit sign on the LHS of Eq. (16) emphasizes additive components of positive pressure *drop* through the bed.

2.1.1.3.2 Shear Forces Acting Within the CV

The classical treatment of fluid flow through the interstices of a porous medium generally involves adopting a well-known solution for internal flow through a cylindrical pipe and then applying a hydraulic scaling argument to account for the complex pathways or "capillaries" through which the water actually passes. The pressure gradient derived for flow in a cylindrical conduit is usually expressed by a differential form of the Hagen-Poiseuille equation as $dP/dz = -8\mu Q/\pi R^4$ where μ is the dynamic viscosity, Q is the volumetric flow rate, and R is the radius of the conduit. One limitation of this approach for the present application is that the above solution is obtained under conditions of uniform longitudinal flow velocity (i.e., no momentum transfer). Thus, the approximate pressure distribution may not be fully coupled to all terms present in the force balance given by Eq. (3).

A derivation of shear forces in a cylindrical capillary is presented next that incorporates the effects of longitudinal acceleration. This section should be viewed as a nested development that treats flow through a single cylindrical conduit rather than as a continuation of the description for bulk flow through the entire bed. The same steady-state force balance described by Eq. (3) will apply, but the momentum, pressure and shear force terms will be modified to express the differential forces per unit of flow-path volume within the capillary. Results describing the pressure gradient for the single conduit will be scaled later to approximate the internal flow complexity and then reintroduced into the bulk flow description to arrive at a correlation for pressure loss through the entire debris bed. Results for the internal pressure gradient are expressed in terms of bed porosity and debris specific-surface area in Section 2.1.2 to obtain a modified version of the Ergun equation for debris-bed head loss.

The immediate objective of this theoretical development is to derive a suitable model for describing pressure losses measured across composite debris beds. It will be shown that viscous shear is a dominant mechanism for inducing pressure drop because the fluid continually loses energy to friction wherever there are velocity gradients. A mental image of continually redirected streamlines within the bed is sufficient to illustrate that cumulative shear stresses must be computed by integrating over the entire volume of the

moving fluid. One longer-term objective is to describe the coupled interaction between hydraulic drag induced by interstitial flow and debris-bed response observed as a bulk thickness reduction. In anticipation of the importance of internal pressure gradients for describing local debris element behavior, gradient representations will be retained for all parameters that may have spatial variations through the bed. Drag occurs at the physical interface between the fluid and the debris elements and may be attributed to both viscous shear in the boundary layer and inertial impaction on the debris elements. These mechanisms of coupling fluid pressure drop to hydraulic drag are discussed in Section 2.1.3.

2.1.1.3.2.1 Derivation of the Viscous-Shear Pressure Gradient

Following the notation of Fox and McDonald (Ref. 13), consider a stationary, differential, annular CV of thickness dr and length dz containing fluid that is moving from left to right within a cylindrical conduit of radius R as shown in Figure 2-3. Given the condition of cylindrical symmetry, the fluid element experiences pressure P and shear stress $\tau_{r,z}$ at radius r. The CV experiences forces F_P^{left} and F_P^{rght} caused by pressure exerted on the left and right annular faces, and it experiences shear stresses F_S^{in} and F_S^{out} on the inside and outside cylindrical surfaces as illustrated. By convention, a shear stress is assigned a positive or negative direction with respect to the longitudinal coordinate that is consistent with the radial direction of the normal vector of the surface on which the stress is acting.

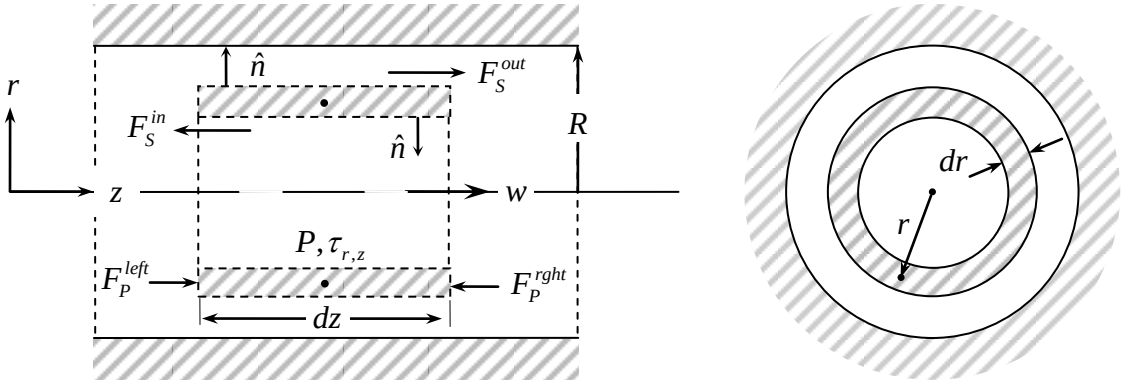

Figure 2-3. Annular control volume used for derivation of shear stress in a cylindrical capillary.

Recall that shear is defined as the force per unit area acting in a direction perpendicular to the surface normal. The shear forces acting within the fluid change as a function of radius and distance, so the desired function $\tau_{r,z}$ is expanded in Taylor's series about the radial midpoint of the differential annular volume. For a CV of constant cross section as shown in Figure 2-3, the shear force acting on the inside cylindrical surface is

$\vec{F}_S^{in} = -\left(\tau_{rz} - \frac{\partial \tau_{rz}}{\partial r}\frac{dr}{2}\right)2\pi\left(r - \frac{dr}{2}\right)dz$ and the shear force acting on the outside cylindrical surface is $\vec{F}_S^{out} = +\left(\tau_{rz} + \frac{\partial \tau_{rz}}{\partial r}\frac{dr}{2}\right)2\pi\left(r + \frac{dr}{2}\right)dz$. Note that the differential areas corresponding to these forces have been evaluated at the inside and outside radii, respectively. The sum of shear forces acting on the CV is

$$\vec{F}_S = 2\pi dr dz\left(\tau_{rz} + r\frac{\partial \tau_{rz}}{\partial r}\right) = 2\pi dr dz \frac{\partial}{\partial r}\left(r\tau_{rz}\right) \tag{17}$$

where products of differential factors have been neglected in the first-order approximation.

Equation (16a) provides the desired form of the shear-induced pressure gradient, but all previous derivations assumed bulk average flow properties across an entire horizontal cross section of the debris bed. The present development of shear stress in a cylindrical capillary considers flow conditions in only one of a multitude of flow paths that exist within the bed. To match the spatial resolution of Eq. (17) to the full bed, we will complete the analysis for a single conduit and scale the result to account for the total internal surface area available to induce shear within the bed. The details of hydraulic scaling will be explained later in Section 2.1.2.

Consider a single cylindrical flow path having an internal velocity profile $w(r,z)$ and differential area $dA = 2\pi r dr$. Using the shear force from Eq. (17), a differential form of (16a) can be written that will be integrated over the total flow area to preserve the average volumetric flow $Q = A\overline{w}$; i.e.,

$$\begin{aligned} -2\pi r dr\left(\frac{dP}{dz}\right)_{Shear} &= (2\rho\beta)2\pi r dr w_{rz}\frac{\partial w_{rz}}{\partial z} - 2\pi dr\frac{\partial}{\partial r}\left(r\tau_{rz}\right) \\ -\left(\frac{dP}{dz}\right)_{Shear} &= (2\rho\beta)w_{rz}\frac{\partial w_{rz}}{\partial z} - \frac{1}{r}\frac{\partial}{\partial r}\left(r\tau_{rz}\right) \end{aligned} \quad . \tag{18}$$

The key to subsequent manipulation of Eq. (18) is the ability to eliminate a common factor of differential area $dA = 2\pi r dr$. It should also be noted that in general, the shear stress and velocity can be functions of both radius and axial location within the capillary as denoted by the subscripts. When comparing the form of the momentum term with previous results, consider Eq. (8) under the assumption that $\partial(A\beta)/\partial z = 0$, which would be true for a perfectly straight conduit of constant cross section, and might be an acceptable approximation if the product $A\beta$ varies slowly. (In reality, impacts of the derivative $d(A\beta)/dz$ are retained in another component of the pressure gradient – see Eq. (16c)). Equation (9) should not be used at this level of spatial resolution, because the volumetric flow rate is not required to be constant over a differential area, only over the conduit-averaged total flow area.

Equation (18) is usually solved for the special case of fully developed flow where the radial velocity profile is constant with position so that $\partial w/\partial z = 0$, and body forces are neglected as would be reasonable for horizontal flow in a pipe. Under these conditions, τ_{rz} is a function of radius only and pressure is a function of position only, so each side of the equation must equal a common constant. Equation (18) thus simplified can be integrated over radial position to obtain

$$\tau_{rz} = \frac{r}{2}\left(\frac{dP}{dz}\right)_{Shear} \tag{19}$$

where the integration constant was set equal to zero to ensure that the shear stress remains finite at the conduit centerline as r approaches zero.

For laminar flow within the capillary, it is true by the definition of dynamic viscosity μ that

$$\tau_{rz} = \mu\frac{dw}{dr}. \tag{20}$$

However, other empirical relations are available for describing radial shear for fully developed turbulent flow in pipes. (See Ref. 13, Section 8-5, for example). In general, turbulent flows will have steeper velocity gradients near the wall than those for laminar flow. If turbulent flow descriptions are incorporated into this derivation at a later time, then the presence of turbulent velocity components should also be added to the definition of the momentum term in the manner described by Ahmed and Sunada (Ref. 2). For now, proceed with the laminar flow definition by substituting Eq. (20) in Eq. (19) and integrating over radius a second time to obtain

$$w(z,r) = -\frac{R^2}{4\mu}\left(\frac{dP}{dz}\right)_{Shear}\left[1-\left(\frac{r}{R}\right)^2\right]. \tag{21}$$

This result is obtained by imposing the boundary condition that $w = 0$ at the wall where the maximum radius $r = R$ is attained.

By conservation of mass, it is true over any cross section of the pipe that $Q = \int_A \vec{V}\cdot d\vec{A} = 2\pi\int_0^R wr\,dr$. In this context, Q represents the total volumetric flow through a single conduit. Substituting Eq. (21) into this relation and integrating over the radius leads to a differential form of the Hagen-Poiseuille equation

$$\left(\frac{dP}{dz}\right)_{Shear} = -\frac{8\mu Q}{\pi R^4}, \tag{22}$$

which can be substituted back into Eq. (21) to obtain the standard form of the parabolic (quadratic) radial velocity profile in a cylindrical pipe

$$w(r,z)=\frac{2Q}{\pi R^2}\left[1-\left(\frac{r}{R}\right)^2\right]. \tag{23}$$

It is important to note that the velocity profile in a debris-bed capillary can retain a dependence on location when the flow-path diameter $D=2R$ is spatially dependent even though the above result was obtained under the assumption of constant flow-path area through a differential length of conduit. The assumption of constant flow area needed to write the differential force balance of Eq. (18) is compensated by the spatially dependent integration limit represented by the conduit radius, so the notational dependence on z will be retained for generality. It is not difficult to visualize a 2-D cylindrical conduit with a varying (or even undulating) radius. The implication of mapping the Eq. (23) velocity profile to a variable radius $R(z)$ is that at any given cross section, the constant volumetric flow is spread in a parabolic velocity distribution over the local flow area.

If the volumetric flow rate is expressed as $Q=\bar{w}A$, then Eq. (22) explains the origin of the "linear" velocity term present in standard correlations of total pressure drop across a debris bed. The linear term is clearly related to pressure losses experienced because of viscous shear within the flow, as emphasized by its proportionality to the dynamic viscosity μ. Traditional expressions for the viscous-shear pressure drop can be obtained by applying to Eq. (22) hydraulic scaling arguments introduced later in this discussion.

One remaining point of possible confusion should be addressed. Viscous shear has been itemized as a force acting on the surface of the fluid CV, but the previous derivation clearly involves integrals over the full volume of the capillary, similar to the approach that would be applied to estimate energy dissipation within the CV. Full volumetric integration is needed because viscosity couples the momentum of the entire fluid medium even though shear is initiated at the contact boundary. For flow in a hypothetical frictionless conduit, no shear can be introduced, and thus, no relative motion can exist between streamlines. By similar reasoning, the full velocity profile within the conduit must transmit the integral of internal shear to the walls where the cumulative force is manifest as a force on the surface of the CV. The previous derivation proceeds in reverse order by distributing the total viscous shear across a parabolic velocity profile. In Section 2.1.3.1 it is demonstrated that the surface shear calculated from the fully developed velocity leads to the same shear-induced pressure gradient derived here.

The preceding development of shear stress and velocity profile in a cylindrical conduit is a familiar presentation in most introductory fluid mechanics text books. However, the results were obtained under idealized conditions that clearly do not hold rigorously for flow through the interstitial gaps of a porous debris bed. These discrepancies are perhaps most evident for highly packed beds with multiple contact points between debris elements. The usual approach taken to accommodate geometric

complexity is to relate the maximum radius of the "pipe" to an equivalent hydraulic radius that accounts for the cumulative effects of all surfaces encountered inside of the debris bed. In this context, viscous shear originating in the boundary layer next to the debris influences the velocity profiles that develop between the elements, and thus, total surface area influences the cumulative degree of viscous dissipation that occurs along all flow paths.

Before appealing to a hydraulic scaling argument, the following discussion proposes a coupled evaluation of Eq. (18) that includes both the momentum and shear forces acting on the fluid element. Though still limited to flow through a single 2-D cylindrical capillary, the refined method approximates the concurrent influence of axial velocity gradients. The purpose of this refinement is to introduce additional detail to the velocity field within the flow channel. Because viscous shear occurs wherever velocity gradients exist, it is hoped that the refined velocity field will provide a more accurate estimate of the viscosity induced pressure gradient.

Equation (18) cannot be integrated over the cylindrical radius to isolate τ_{rz} in the manner illustrated earlier unless a radial velocity profile is available to define $w(r,z)$. Although the result was derived for somewhat different flow conditions, Eq. (23) probably captures the radial dependence to an approximation adequate for initializing an analytic iteration on the derivation of interstitial shear stress in the presence of axial velocity gradients. When substituting Eq. (23) into Eq. (18) and performing the first integration over radius, the principal difficulty will be encountered with the momentum term, so the evaluation is presented here in some detail. Throughout this derivation, it is assumed that the flow-path area retains a dependence on location as parameterized by $R(z)$. Consider the following integration

$$
\begin{aligned}
2\rho\beta\int rw\frac{\partial w}{\partial z}\,dr &= 2\rho\beta\int r\left[\left(\frac{2Q}{\pi}\right)^2\left(\frac{1}{R^2}-\frac{r^2}{R^4}\right)\frac{d}{dz}\left(\frac{1}{R^2}-\frac{r^2}{R^4}\right)\right]dr \\
&\vdots \\
&= \left(\frac{8\rho\beta Q^2}{\pi^2}\right)\left(2R^{-5}\frac{dR}{dz}\right)\int\left(-r+3r^3R^{-2}-2r^5R^{-4}\right)dr \\
&\vdots \\
&= \frac{16\rho\beta Q^2}{\pi^2R^5}\left(-\frac{r^2}{2}+\frac{3r^4}{4R^2}-\frac{r^6}{3R^4}\right)\frac{dR}{dz}+C_1.
\end{aligned}
$$

Substitute this result into a complete radial integral of Eq. (18) and continue the integration term by term to obtain

$$\tau_{rz} = \frac{16\rho\beta Q^2}{\pi^2R^5}\left(-\frac{r}{2}+\frac{3r^3}{4R^2}-\frac{r^5}{3R^4}\right)\frac{dR}{dz}+\frac{r}{2}\left(\frac{dP}{dz}\right)_{Shear} \tag{24}$$

where the integration constant must be set equal to zero to hold τ_{rz} finite as $r \to 0$. Note the reappearance of Eq. (19) and a correction term related to the spatial gradient of the flow path.

Now, the definition of shear stress under laminar flow from Eq. (20) can be substituted to obtain a force-coupled expression for the velocity profile. Had the original development been performed using turbulent flow correlations, then it would be prudent to use the same expressions at this point of the refinement as well. Substitution of Eq. (20) into Eq. (24) and integration over the radius yields $w = \frac{16\rho\beta Q^2}{\mu\pi^2 R^5}\left(-\frac{r^2}{4}+\frac{3r^4}{16R^2}-\frac{r^6}{18R^4}\right)\frac{dR}{dz}+\frac{r^2}{4\mu}\left(\frac{dP}{dz}\right)_{Shear}+C_2$. When $r = R,\ w = 0,$ so the integration constant is found to be $C_2 = \frac{16\rho\beta Q^2}{\mu\pi^2 R^3}\left(\frac{17}{144}\right)\frac{dR}{dz}-\frac{R^2}{4\mu}\left(\frac{dP}{dz}\right)_{Shear}$. Substitution and simplification yields the velocity profile

$$w(r,z) = \frac{16\rho\beta Q^2}{\mu\pi^2 R^3}\left[\frac{17}{144}-\frac{1}{4}\left(\frac{r}{R}\right)^2+\frac{3}{16}\left(\frac{r}{R}\right)^4-\frac{1}{18}\left(\frac{r}{R}\right)^6\right]\frac{dR}{dz}+\frac{\left(r^2-R^2\right)}{4\mu}\left(\frac{dP}{dz}\right)_{Shear}. \quad (25)$$

There is no inherent reason why Eq. (25) cannot be substituted back into Eq.(18) and the analytic derivation iterated to obtain yet a better estimate of the force-coupled shear stress. One might expect the polynomial approximation to improve and eventually reach a theoretical limit that represents a converged solution of the differential equation, but no proof of this conjecture is offered at this time. Two convenient features of this analytic iteration are that (1) it involves only polynomial integration and (2) all dependence on the internal radius r collapses to a constant when either integrated over the range from 0 to R or evaluated at $r = 0$ or $r = R$. In particular, $w(r = R, z) = 0$ at all z. One unfortunate complication of successive iteration would be the appearance of higher derivatives like d^2P/dz^2 and d^2R/dz^2.

For now, evaluate the volumetric flow rate through the conduit, $Q = \int_A \vec{V}\cdot d\vec{A} = 2\pi\int_0^R wr\,dr,$ to eliminate dependence on the internal radius r. Integration of Eq. (25) and simplification leads to a generalized form of the Hagen-Poiseuille equation for the pressure gradient along an individual idealized cylindrical conduit,

$$\left(\frac{dP}{dz}\right)_{Shear} = \frac{16\beta Q^2}{3\pi^2 R^5}\left(\frac{dR}{dz}\right)\rho-\frac{8Q}{\pi R^4}\mu. \quad (26)$$

For the sake of completeness, substitute Eq. (26) back into Eq. (25) and regroup to obtain a final form of the refined velocity profile,

$$w(r,z)=\frac{16\rho\beta Q^2}{\mu\pi^2 R^3}\left[\frac{5}{144}-\frac{1}{6}\left(\frac{r}{R}\right)^2+\frac{3}{16}\left(\frac{r}{R}\right)^4-\frac{1}{18}\left(\frac{r}{R}\right)^6\right]\frac{dR}{dz}+\left[1-\left(\frac{r}{R}\right)^2\right]\frac{2Q}{\pi R^2} \qquad (27)$$

Equation (26) captures the principal dependencies of the pressure gradient within a single flow-path conduit, and to a large extent, pressure gradients throughout the entire debris bed. Several features of this result deserve further description:

- First, the first RHS term of the equation carries a quadratic dependence on velocity (seen explicitly when substituting $Q=\bar{w}A$) that arises from momentum changes inside the bed, but this quadratic dependence is *not* the same as that included in traditional head-loss correlations in association with inertial drag. Note that there will be no net momentum change if there is not a spatial gradient to induce acceleration in the velocity field. Here, the gradient is expressed as dR/dz denoting a spatial variation in the effective flow-path diameter. Spatial variations can occur exclusively at the inlet and outlet faces of the bed, or continuously throughout the porous medium.
- Second, the sign of the momentum term is properly controlled by the spatial gradient. If the flow-path is becoming restricted in the direction of flow $(dR/dz<0)$ then the pressure declines more rapidly because fluid velocity must increase. If the flow path is expanding, for example, at the exit face, then the pressure declines less rapidly. The simple observation that net pressure losses are always experienced across a debris bed rather than pressure gains suggests that the second term representing viscous shear dominates any small increases that can be attributed to gravity with increasing depth through the relatively small bed thickness, and that net pressure variations caused by momentum changes at the inlet and exit faces may be negligibly small, if not identically zero. The momentum term may still be necessary for describing the internal distribution of forces that contribute to compression and compaction, however.
- Third, while there was no explicit dependence of flow-path area on position built into the differential force balance of Eq. (18) as there was earlier for the macroscopic bed description, there is no apparent reason why the flow-path radius R in this submodel cannot be treated as a function of location in the bed. This is an acknowledged approximation of the derivation that might be remedied by expanding the radial dependence of R along the z dimension of the CV, but then the mechanics of solving the force-coupled equations are not at all obvious.
- Fourth, the observation that the viscous term appears unchanged from the original derivation, which assumed steady flow (compare Eqs. (22) and (26)), suggests that the preceding iteration process has yielded a physically realistic equation. This fact also suggest that no mathematical coupling actually exists between the shear stress and the developing velocity profile under this approximation and that there may be a more direct solution path to the same result. Separability of radial shear from the axial velocity gradient further

rationalizes the separate treatment of inertial drag as a supplementary surface force that can be added to the local pressure gradient.

- Finally, the result obtained strictly applies only to an idealized 2-D cylindrical flow geometry, and it must be scaled in some fashion to account for complex flow patterns within a porous medium.

One implication of Eq. (26) may be particularly relevant to the interpretation of experimental data if it can be shown that a similar form applies for the total pressure gradient throughout the entire debris mat. The primary enterprise of most head-loss experiments is to measure the total pressure drop experienced across a debris bed of some uniform thickness; and, generally speaking, pressure taps are placed well upstream and downstream of the bed to avoid the velocity transition zones and ensure accurate, stable measurements. Considering only viscous shear, axial momentum changes, and gravity (added to the formula temporarily) as an example, the total pressure difference between measurement taps located at positions z_1 and z_4 across a bed beginning at z_2 and ending at z_3 can be predicted by integrating Eq. (26) along the direction of flow in the following manner

$$\int_{z_1}^{z_4} dP = \frac{16\rho\beta Q^2}{3\pi^2}\int_{z_1}^{z_4}\frac{dR}{R^5} + \int_{z_1}^{z_4}\left(\rho g - \frac{8}{\pi}\frac{Q}{R^4}\mu\right)dz,$$

$$P_4 - P_1 = -\frac{4\rho\beta Q^2}{3\pi^2}\frac{1}{R^4}\Bigg|_{R(z_1)}^{R(z_4)} + \rho g\left(z_4 - z_1\right) - \frac{8}{\pi}Q\mu\int_{z_1}^{z_4}\frac{dz}{R^4\left(z\right)},$$

$$\Delta P = \rho g\left(z_4 - z_1\right) - \frac{8}{\pi}Q\mu\int_{z_1}^{z_4}\frac{dz}{R^4\left(z\right)}. \qquad (28)$$

The key finding of this exercise is that the quadratic-velocity momentum term vanishes because the flow path areas, and thus the fluid velocities for constant volumetric flow, are identical at the locations of the pressure taps. Contributions of momentum change to a measured pressure difference are determined by conditions at the observation points and not by the path integral between the points. Only a few experimental studies have actually obtained direct measurements of pressure within the body of a relatively thick debris bed where this observation might be critical for proper data interpretation (Ref. 16). In most cases, pressure-tap data are obtained across the entire bed in a constant cross section apparatus under conditions of approximately constant flow, and the net momentum change is zero.

Equation (28) also reminds that gravitational effects must be compensated or subtracted from any measurements that are intended to report pressure differences attributably directly to the presence of the debris bed. Gravitational pressure differences do not result from any characteristic of the flow or the debris because they simply represent the static weight of the water column between pressure transducers. Similarly, gravitational pressure differences do not contribute to compression or compaction of the bed because continuous fluid surrounds every internal structure and transmits the weight

of the column to adjacent fluid elements on a much finer spatial scale than that of the solid debris, which cannot be deformed under small pressure gradients exerted over distances comparable to their size.

2.1.2 Modified Ergun Equation

The preceding development of shear stress in an idealized cylindrical capillary represents a microscopic flow perspective that must be aggregated or scaled to the physical proportions of the debris bed in order to accurately describe pressure drops incurred across complex porous media. This scaling is traditionally accomplished by introducing a "hydraulic radius" to substitute for the dimensional parameter R that preserves the "similitude" of the problem. Essentially, a spatial integration must be performed to add up the head-loss contributions of all complex flow paths occurring through the bed; but, because the internal geometry cannot be known with infinite detail and because the derivation of pressure gradients in a capillary holds only for simplistic flow configurations, an effective integration is performed using the following heuristic argument.

Velocity gradients develop in interstitial flow because the viscosity of the fluid couples friction at the surface of the debris elements where the velocity approaches zero to the free-field flow where velocities are maximum. Thus, while viscous energy dissipation is distributed throughout the fluid volume, it is initiated at the surface of the conduit through which the fluid travels. As internal surfaces become more complex, surface friction has a greater influence on the velocity field and viscous pressure losses increase. This intuitive argument is captured by the following ratio, which is defined as the hydraulic radius;

$$R_H = \frac{\text{flow volume}}{\text{wetted surface area}}. \tag{29}$$

Choosing meaningful definitions of the "flow volume" and the "wetted surface area" is not as simple as it may sound for some complex media. Of course, it is traditional to assume that the entire free volume is flowing and that liquid moves in equal contact across the entire surface area of all debris elements, but there are exceptions that have been noted in the literature and empirical compensations that have been made to achieve better agreement between theory and observation. Compared to the smooth internal flows that were presumed in the capillary derivation, flow through a porous bed experiences lee-wake eddies, vortex separation at sharp boundaries, complex rotation, flow stagnation in dead cavities, surface tension and air occlusion of micropores, and nonuniform spatial accelerations. In fact, some investigators (Ref. 10) have achieved some success using analytic approximations of shear stress developed for external flow over regular objects like rods and spheres and then integrating these effects into a composite flow field using scaling arguments much like the hydraulic radius defined in Eq. (29). Corrections of this nature often appear in the published head-loss formulas as functional combinations of geometric properties like porosity with exponents either fractional or shifted by an integer compared to the classical derivations based on regular debris elements like spheres and cylinders.

For a cylindrical pipe, and hence for an idealized interstitial flow path, the hydraulic radius is $R_H = \pi R^2\, dz / 2\pi R\, dz = R/2$, so $R = 2R_H$ and $dR/dz = 2\,dR_H/dz$. To facilitate the substitution of R_H in Eq. (26), first express the total interstitial flow area as $A = \pi R^2$ and use the definition $Q = \overline{w}A$ to make the velocity explicit. Finally, substitute the above definitions to obtain

$$\left(\frac{dP}{dz}\right)_{Shear} = \frac{16\beta}{3R_H}\left(\frac{dR_H}{dz}\right)\overline{w}^2\rho - \frac{2}{R_H^2}\,\overline{w}\mu\,. \tag{30}$$

Recall that $\overline{w}$ denotes the interstitial vertical flow velocity averaged over lateral variations in the one-dimensional bed and that Q is the bulk volumetric flow velocity. This is a more significant approximation than it might first appear. Throughout the previous section, the microscopic perspective of flow in a single capillary permitted the interpretation of Q as the "local" volumetric flow that was then distributed over the local flow area in a parabolic velocity distribution. Now, the perspective has shifted back to the attributes of the aggregate bed, and it is implicitly assumed that every representative conduit carries the same bulk flow as the bed average. There is no fundamental reason why this should be strictly true, which suggests a possible future refinement from a single average conduit to a distribution of local flow conditions.

Inside of a porous debris bed, the volume fraction that is open for water to pass through is defined by the porosity ε. The complement of porosity, or the solidity $(1-\varepsilon)$, is the volume fraction of the bed occupied by debris elements. The total surface inside of the bed that is exposed to wetting is characterized by the specific surface area S_V, which is defined as the debris surface area per unit of solid debris volume with units of $\{m^2/m^3\} = \{m^{-1}\}$. For example, for a spherical particle of diameter D_P, $S_V = 4\pi(D_P/2)^2 / (4\pi/3)(D_P/2)^3 = 6/D_P$. Given these conventions, the hydraulic radius of a complex debris bed can be expressed by considering a typical unit volume $\forall$;

$$R_H = \frac{\text{water volume}}{\text{debris area}} = \frac{\varepsilon\forall}{(1-\varepsilon)\forall S_V} = \frac{\varepsilon}{(1-\varepsilon)S_V} \tag{31}$$

where both ε and S_V are functions of depth through their dependence on fiber and particulate mass distributions that may exist in a nonuniform debris bed. Remember that this definition of hydraulic radius assumes perfectly uniform contact between the continuously moving fluid and the debris-element surfaces.

Through the definition of porosity is also obtained a relationship between the interstitial flow area and the approach area of the screen $A\,dz = \varepsilon A_A\,dz$, or $A = \varepsilon A_A$; and because the volumetric flow rate is constant through the bed and upon approach, $\overline{w}A = Q = w_A A_A$, or $\overline{w}\varepsilon A_A = w_A A_A$, which relates the interstitial and approach velocities as $\overline{w} = w_A/\varepsilon$. Head-loss formulas are often expressed in terms of the approach velocity

because it can either be measured directly or it can be derived from a measured volumetric flow rate using a known flow area upstream of the debris bed.

Before substituting these definitions of hydraulic radius and approach velocity in Eq. (30), evaluate the spatial derivative of the hydraulic radius to obtain $\frac{dR_H}{dz} = \frac{R_H}{\varepsilon}\frac{d\varepsilon}{dz} - \frac{R_H^2}{\varepsilon}\left[(1-\varepsilon)\frac{dS_V}{dz} - S_V\frac{d\varepsilon}{dz}\right]$. Now, substitution and simplification offers the final result that

$$-\left(\frac{dP}{dz}\right)_{Shear} = 2\frac{(1-\varepsilon)^2}{\varepsilon^3}S_V^2\mu w_A + \frac{16\beta}{3}\left(\frac{1-\varepsilon}{\varepsilon^3}\right)\left[\frac{\varepsilon}{(1-\varepsilon)S_V^2}\frac{dS_V}{dz} - \frac{1}{S_V(1-\varepsilon)^2}\frac{d\varepsilon}{dz}\right]S_V\rho w_A^2 . \quad (32)$$

The second term of Eq. (32) has been factored to facilitate comparisons with traditional head-loss formulas. For example, Ergun (Ref. 12) reports a composite formula of the form

$$\frac{\Delta P}{L}g_c = 150\frac{(1-\varepsilon)^2}{\varepsilon^3}\frac{\mu U_m}{D_P^2} + 1.75\left(\frac{1-\varepsilon}{\varepsilon^3}\right)\frac{GU_m}{D_P} \quad (33)$$

where L is the bed thickness, ΔP is the positive pressure *reduction* from the top of the bed to the bottom, g_c is the gravitational force constant ($g_c = 1$ when all other quantities are specified in SI units), $D_P = 6/S_V$ is an effective spherical particle diameter, U_m is the approach velocity measured at the average pressure, and $G = \rho U_m$ is the mass flux. Making minor substitutions for g_c, D_P and G in Eq. (33) brings the two equations closer in form; i.e.,

$$\frac{\Delta P}{L} = \frac{25}{6}\frac{(1-\varepsilon)^2}{\varepsilon^3}S_V^2\mu U_m + \frac{1.75}{6}\left(\frac{1-\varepsilon}{\varepsilon^3}\right)S_V\rho U_m^2, \quad (34)$$

but it does not resolve several important differences.

The following comparison discusses many of the differences between Eqs. (32) and (34):

- Ergun developed much of his work to describe gas flow through porous beds. This may explain why there is a measurement of bulk flow U_m taken at the "average" pressure and why the contribution of gravity was not important for obtaining successful correlations with data. For liquid flow, it will be assumed that $U_m = w_A$. It should also be noted that much of Ergun's data was obtained in regimes of industrial mass flow rate that are much higher than those needed to study typical water penetration of ECCS-sump-screen debris beds. Also, it is noted that gas viscosity increases with temperature in contrast to liquid viscosity.

Presumably the data were interpreted using accurate evaluations of the fluid properties.

- The Ergun equation contains an increased factor of approximately 2 in the coefficient of the first term that may have arisen for several reasons: (a) perhaps there is a difference in the approximations used for flow-area integration in the fundamental differential equations, (b) perhaps different definitions of hydraulic radius were adopted, (c) perhaps the debris elements largely studied by Ergun do not fit the assumption imposed by this derivation of full contact between the solid debris surface and the moving fluid. While this difference may appear minor, it translates directly into a factor of 2 discrepancy between any material properties that are inferred from pressure-loss data using the two formulas. Observations are offered in Section 2.1.3.2 to explain why the coefficient derived for Eq. (32) may underestimate the effects of viscous head loss compared to Ergun's measurements.

- The most obvious differences between the two formulas lie in the quadratic-velocity (second) terms. First, it is important to understand that the two terms are not intended to describe the same phenomena. Equation (32) explicitly enforces the requirement that a spatial gradient be present in order to experience any acceleration that can induce a change in momentum giving rise to second-order forces. Equation (34) neglects the possibility of net acceleration across the bed presumably because of the constant-cross section, constant-volumetric-flow experimental configuration. The quadratic term in the Ergun equation arises from high-velocity inertial drag that will be discussed in Section 2.1.3.2. A comparison of results to Eq. (34) will be offered at that time.

- In some sense, the Ergun formula predicts the average pressure gradient across the entire bed because the correlation is expressed in terms of the total pressure drop divided by the total bed thickness. Equation (32) will be manipulated to imitate this averaging process and perhaps resolve some of the largest disparities between the two formulas.

- Upon integration of Eq. (32) over the distance between pressure taps to predict the total head loss, it is found that the momentum term vanishes because the material properties of ε and S_V return to their respective original values of 1 and 0 after the fluid passes through the bed. This behavior of Eq. (32) when compared to the proven success of the Ergun equation suggests that inertial drag can be an important alternative source of quadratic-velocity dependence in the pressure gradient for some flow regimes.

Integration of Eq. (32) (with gravity included for comparison) between pressure taps located at z_{top} and z_{bot} across the bed of thickness L leaves a total pressure drop of

$$-\left(P_{bot}-P_{top}\right)\equiv\Delta P=2\mu w_A\int_{top}^{bot}S_V^2\frac{\left(1-\varepsilon\right)^2}{\varepsilon^3}\,dz-\rho g\left(z_{bot}-z_{top}\right). \tag{35}$$

(Recall that the z coordinate is directed downward for this derivation). If the material properties are constant through the bed of thickness L and $\varepsilon=1$ elsewhere, then

$$\Delta P=2\mu w_A S_V^2\frac{\left(1-\varepsilon\right)^2}{\varepsilon^3}L-\rho g\left(z_{bot}-z_{top}\right), \tag{36}$$

and the bed-averaged pressure drop is

$$\frac{\Delta P}{L}=2\mu w_A S_V^2\frac{\left(1-\varepsilon\right)^2}{\varepsilon^3}-\rho g\frac{z_{bot}-z_{top}}{L}. \tag{37}$$

Typically, pressure transducers tapped on opposite sides of a debris bed will be compensated to read zero differential pressure under zero flow, thus accounting for the static pressure difference between them. In this case, the gravitational term is not needed to discuss flow-induced pressure changes across the bed. Comparison of the first terms appearing in Eqs. (34) and (37) reveals a factor of ~2 discrepancy between the present derivation and the traditional Ergun formulation.

Other investigators have used empirical evidence and semitheoretical arguments to optimize the first term of Eq. (32) for better agreement with particular filter media. For example, Davies (Ref. 10) reports for long cylindrical filter elements (like fiberglass) a linear-velocity pressure gradient of the form $3.5\left(1-\varepsilon\right)^{1.5}\left[1+57\left(1-\varepsilon\right)^2\right]S_V^2\mu w_A$. This form represents a significant departure from the classical Ergun equation in its dependence on porosity, but it provides an optimized description for data taken in a filter media very similar to fiberglass insulation debris. For this reason, the Davies representation of linear-velocity pressure gradients was adopted by Rao for use in Ref. 43. With a predominance of high particulate-to-fiber ratios in the STP accident space causing the most concern for potential strainer head loss, and extremely low approach velocities, the standard factorization that is more typical of granular beds will be carried forward here.

2.1.3 Hydraulic Drag

Comparisons of bed-averaged pressure loss formulas obtained thus far to the classic Ergun equation have noted the absence of a term that is proportional to the square of the approach velocity, the so-called “quadratic head-loss” effect. This term is often included in a semitheoretical manner to account for the dominance of inertial drag in high-velocity flow regimes, and this is why the list of surface forces acting on a fluid CV itemized in

Section 2.1.1.3 included the possibility of momentum transfer by direct flow impingement on debris elements. This effect is categorized as a surface force because no fluid actually crosses the CS; a mental image of molecular impingement and redirection is helpful to understand the concept of momentum transfer from the fluid to the solid debris. While it might be true that all migrating fluid moves parallel to the surface of the debris under the approximation of zero-velocity surface flow in a well-developed boundary layer, in many practical conditions, fluid that is diverted around a debris element experiences a significant change in momentum that is transferred to the obstacle through a process described here as inertial drag. Precise calculations of momentum exchange cannot be made without detailed information about the velocity field similar to the information that is rolled up in the β flow-diversion factor, so the extra term is "added on" to the correlation to accommodate behavior that is observed in the limit of high-velocity flow. Earlier, an additive force balance was defined to anticipate introduction of various phenomena, but the definitions of each component are somewhat arbitrary and do not follow from first principles.

It will be shown in Section 2.1.3.1 that viscous shear also imparts drag forces on the internal surfaces of the fluid CV that are proportional to the product of dynamic viscosity and local average velocity $\mu\bar{w}$, but inertial drag discussed in Section 2.1.3.2 imparts forces that are proportional to the product of the fluid density and the local velocity squared $\rho\bar{w}^2$. Satisfactory predictions of head-loss can be obtained for many debris beds by considering only the viscous effects and by neglecting quadratically dependent inertial drag entirely. The success of this approximation indicates that forces induced by inertial momentum transfer will seldom compete with viscous shear in the flow regimes applicable to sump-screen blockage by composite debris beds. Because high-velocity flow regimes are rarely encountered in sump-screen head-loss applications, the presence of a quadratic pressure gradient term that is not tightly integrated into the theoretical derivation can cause difficulties when interpreting data that falls in the transition between velocity regimes. This difficulty has lead a number of investigators to propose geometric corrections to the coefficients of both the linear and the quadratic-velocity terms in order to achieve better agreement with specific compositions and arrangements of debris-bed elements in the velocity ranges of interest.

Experimentalists who have experience fitting quadratic models to measured data often complain about ill-behaved extrapolations and the relatively small values assigned to the quadratic coefficients, so it may be that observations of nonlinear pressure drop with increasing flow velocity are more likely to be caused by bed compression and compaction that reduce porosity rather than by the effects of inertial drag. However, if head-loss data are collected at higher velocities for the sole purpose of determining hydraulic resistance properties of various debris materials, then it is important that a quadratic correlation like Eq. (34) be implemented.

In the following two sections are described two aspects of hydraulic drag. First, in Section 2.1.3.1 is verified a component of the drag force that is already inherent to viscous coupling of shear induced near the debris surface. Then, a derivation of the classic quadratic-velocity inertial drag component is presented in Section 2.1.3.2.

Because the quadratic term is simply added on to the formula to compensate for observed pressure-loss trends at high velocity rather than derived as a member of the coupled force balance, it will become apparent that some duplication exists between the two sources of drag. Each represents a different extreme of flow velocity, and some refinements may be needed to smooth the transition between the competing linear and quadratic terms.

2.1.3.1 Drag Imparted by Fluid Shear

Shear work is performed throughout the body of flowing water because velocity gradients in the flow require that fluid layers "slip" past one another, expending thermodynamic pressure to overcome the viscous effects of molecular friction. Viscous coupling conveys all of this friction to the surface of the debris in a manner that can exert drag capable of moving debris elements or causing compression within the bed. This fact was incorporated in the previous derivation of shear-induced pressure gradient by evaluating velocities and shear stress at the full capillary radius R before scaling to the hydraulic equivalent surface area. This section confirms that drag imparted on debris elements is equal in magnitude and opposite in direction to the viscous shear imparted on a fluid element.

On a microscopic scale, the process of momentum transfer between a moving fluid and the intricate surface of a debris element involves complex phenomena and practically infinite geometric detail. However, it is usually sufficient to assume the existence of a boundary layer where fluid in contact with the solid surface moves with a velocity that is essentially zero compared with fluid only a few molecular layers deeper into the free stream. This zero-velocity boundary condition was imposed in the derivation of the radial velocity profile inside of a cylindrical capillary. While the fluid velocity may approach zero at the debris surface, the velocity gradient is *not* required to equal zero; and because the shear stress $\tau = \mu\left(\partial w/\partial r\right)$, the gradient can be evaluated at the wall to estimate the shear stress that fluid moving in the boundary layer imparts to the debris surface.

The classical parabolic radial velocity distribution in a cylindrical pipe of radius R carrying volumetric flow Q was given by Eq. (23). The radial derivative of that distribution is $\frac{dw}{dr} = -\frac{4Q}{\pi R^4} r$, and when the derivative is evaluated at the maximum radius and substituted into the shear stress distribution, the resulting formula is

$$\tau\left(r = R\right) = -\frac{4Q\mu}{\pi R^3}. \tag{38}$$

Recall that this is the shear stress imposed on fluid in the CV near the boundary, so the coupled force on the wall acts in the opposite direction, i.e., in the direction of fluid motion. The drag force acting on a differential length of the capillary is $dF_{Drag} = -\tau dA_{wall}$ where $dA_{wall} = 2\pi R\, dz$. Substituting $Q = w_A A_{flow}/\varepsilon$ and expanding the area in terms of R leads to the final result for the differential force acting *on* the debris in the direction of flow,

$$dF_{Drag} = \frac{8\pi}{\varepsilon(z)} \mu w_A \, dz. \tag{39}$$

The differential pressure loss induced *on* the fluid from internal drag is then obtained by averaging the drag force over the flow area and scaling a single capillary by the effective hydraulic radius to obtain

$$-\left(\frac{dP}{dz}\right)_{Drag} = 2\frac{(1-\varepsilon)^2}{\varepsilon^3} S_V^2 \mu w_A .$$

As expected, this is the same result as obtained for the first term of the pressure gradient from shear losses. This exercise confirms that the original derivation of shear loss was properly evaluated by applying the full effect of viscous coupling at the surface of the capillary.

This same procedure can be generalized using the refined velocity distribution given by Eq. (27). The formula can be differentiated with respect to r and evaluated at $r = R$ to obtain $\left.\frac{dw}{dr}\right|_R = \frac{4\rho\beta Q^2}{3\mu\pi^2 R^4}\frac{dR}{dz} - \frac{4Q}{\pi R^3}$. The corresponding differential drag needed to predict local bed response is found, after substitution and simplification, to be

$$dF_{Drag} = -\left(\frac{32\pi\beta}{3}\rho w_A^2 \frac{R_H(z)}{\varepsilon^2(z)}\frac{dR_H}{dz} - \frac{8\pi}{\varepsilon(z)}\mu w_A\right)dz \tag{40}$$

Further substitutions can be made in the first term of the RHS of Eq. (40) to express the hydraulic radius R_H in terms of the porosity and specific surface area, but it is important to note that this term will only be nonzero for spatial intervals where a net gradient exists in the debris properties. Across the entire bed there will be no net contribution from the first term to the cumulative drag force, so the first term may be relevant only for assessing local effects on debris elements that can migrate. In other words, the first term may be important for describing compaction phenomena and not for uniform mechanical compression. If Eq. (40) is scaled and averaged over the flow area, the shear-induced pressure gradient of Eq. (32) is reproduced as expected.

The viscous component of drag acting on the debris elements is initiated by fluid moving in the boundary layer very close to the debris surface, but it fully couples all viscous shear occurring throughout the moving fluid. Viscous drag may only play an important role in the Stokes-flow regime where viscosity dominates inertial flow effects, i.e., very low Reynolds numbers. A full development of Stokes' law for the drag force exerted by external flow on a spherical particle is given at the end of Chapter 3 in Ref. 15 The approach implemented here to derive the differential drag for internal flow in a debris bed is similar. In the next section, the drag force for inertia-dominated flow is

explored to explain the origin of the quadratic-velocity term present in the Ergun equation.

2.1.3.2 Drag Imparted by Inertial Transfer

Hinds (Ref. 15) presents the following derivation of Newton's resistance law, which is the fundamental basis for the quadratic-velocity term in the Ergun head-loss correlation. Newton derived a general equation for the force resisting the motion of a body through a fluid as part of a ballistic evaluation of cannonball trajectories. He reasoned that the drag imparted to the object must be proportional to the acceleration of the fluid that has to be pushed aside as the body passes through. For a spherical body moving through a stationary fluid at constant velocity $\bar{w}$, or equivalently, a fluid moving around a stationary sphere, the rate of mass displacement equals the cross sectional area of the body times the velocity times the density within the displaced volume, i.e., $\dot{m} = \rho \frac{\pi}{4} d^2 \bar{w}$. The acceleration of the displaced fluid is proportional to the relative velocity between the body and the fluid so $\frac{\text{change of momentum}}{\text{unit of time}} \propto \dot{m}\bar{w} = \rho \frac{\pi}{4} d^2 \bar{w}^2$. Thus, the force required to move the body through the medium, or equivalently, the drag exerted on the body as the fluid passes around it is given by $F_D = K\rho \frac{\pi}{4} d^2 \bar{w}^2$ where K is a constant of proportionality. Experimental investigation shows that the proportionality between drag force and momentum change is only approximately constant for spherical-particle Reynolds numbers $Re > 1000$, so a more general convention is adopted by introducing a drag coefficient that can be correlated as a function of *Re*. Thus, the standard convention is

$$F_D = \frac{1}{2} C_D\left(Re\right) \frac{\pi}{4} \rho d^2 \bar{w}^2 . \tag{41}$$

Discussions of external flow around objects generally assume that the relevant value of Reynolds number is defined by the characteristic diameter of the particle. This is true of information presented in this section as well, but prior to this discussion of drag, the physical model being developed was supported by a mental image of internal flow within a cylindrical capillary where the characteristic dimension was assumed to be the hydraulic radius $R_H = R/2$. It is helpful to have a relationship between the two definitions of Reynolds number applying to each of these cases that is stated in terms of the macroscopic debris-bed properties. For internal flow within an idealized channel,

$$Re_f = \frac{\rho}{\mu} \bar{w} R_H = \frac{\rho w_A}{\mu \varepsilon} \frac{\varepsilon}{\left(1-\varepsilon\right) S_V} = \frac{\rho w_A}{\mu \left(1-\varepsilon\right) S_V} . \tag{42}$$

For a spherical particle, $S_V = 6/D_p$, so $Re_f = \dfrac{D_p \rho w_A}{6\mu(1-\varepsilon)}$. Thus, Reynolds number for a spherical particle can be written as $Re_p = \dfrac{\rho w_A}{\mu\varepsilon} D_p = 6\dfrac{(1-\varepsilon)}{\varepsilon} Re_f$. This result implies that $Re_p = Re_f$ for beds of spherical particles with $\varepsilon \approx 0.86$. When $\varepsilon \approx 0.75$, the particle Reynolds number is twice as large as that for the flow, and when $\varepsilon \approx 0.92$, the flow Reynolds number is two times larger than that for the particle. For typical fiber-bed porosities in the range of $\varepsilon \approx 0.9$, the flow Reynolds number is ~1.5 times larger than the particle Reynolds number.

At a temperature of 60ºC, water viscosity and density are 4.664×10^{-4} Pa-s and 983.2 kg/m^3, respectively (Ref 14). Assuming a nominal 10-μm diameter particle (similar to the diameter of fiberglass strands), and a bed porosity of 0.9 leads to $Re_p = (23.4\,\mathrm{s/m})\,\bar{w}_A$. Typical approach velocities for sump screens range from 1.5×10^{-3} to 3.05×10^{-2} m/s (0.005 to 0.1 ft/s), so expected Reynolds numbers for the debris elements range from 3.5×10^{-2} to 0.71. Flow Reynolds numbers for the same conditions range from 5.25×10^{-2} to 1.07. For the convenience of reading Ergun's paper (Ref. 12), these ranges convert to $0.3 \le \dfrac{N_{Re}}{1-\varepsilon} \le 6.4$ where $N_{Re} = D_p \rho w_A / \mu$.

Equation (41) was derived based solely on the inertia of the displaced fluid so it will only be completely valid for high Reynolds numbers where inertial forces dominate viscous forces. It was also derived assuming complete normal incidence of the fluid across the face of the object, as one would imagine for a flat-faced cylindrical billet rather than for a sphere. This assumption maximizes the lateral fluid acceleration needed to achieve the displacement volume created by relative motion of the body through the velocity field. Common experience with projectiles suggests that optimized shapes can be designed to minimize drag for the same maximum cross sectional area. Also, the fundamental concept of a single object moving through an external flow is immediately challenged by the complex internal flow paths of a composite debris bed. For these reasons, it is not difficult to understand why debris/filter shape factors and complicated correlations have been developed to improve the performance of Eq. (41) for describing drag effects through porous beds.

Figure 2-4 illustrates the empirical behavior of the drag coefficient for several standard debris-element geometries over a wide range of Reynolds number. In the Stokes-flow limit where $Re_p < 1$, $C_D = 24/Re_p$ for flow over a single spherical particle. A numerical check of Figure 2-4 reveals an empirical fit of $C_D \approx 29.44/Re_p$ for a bed of spherical objects. The 23% increase in the numerical coefficient could easily be accommodated by explicitly factoring the porosity ratio and the specific surface area from the trend in the manner of Eq. (32). The approximately constant value of drag in the range $100 < Re < 200{,}000$ for cylindrical objects reaffirms the linear addition of viscous

shear and inertial drag. The data support a relatively small but stable base of inertial drag to which viscous shear becomes an additive effect at lower *Re*.

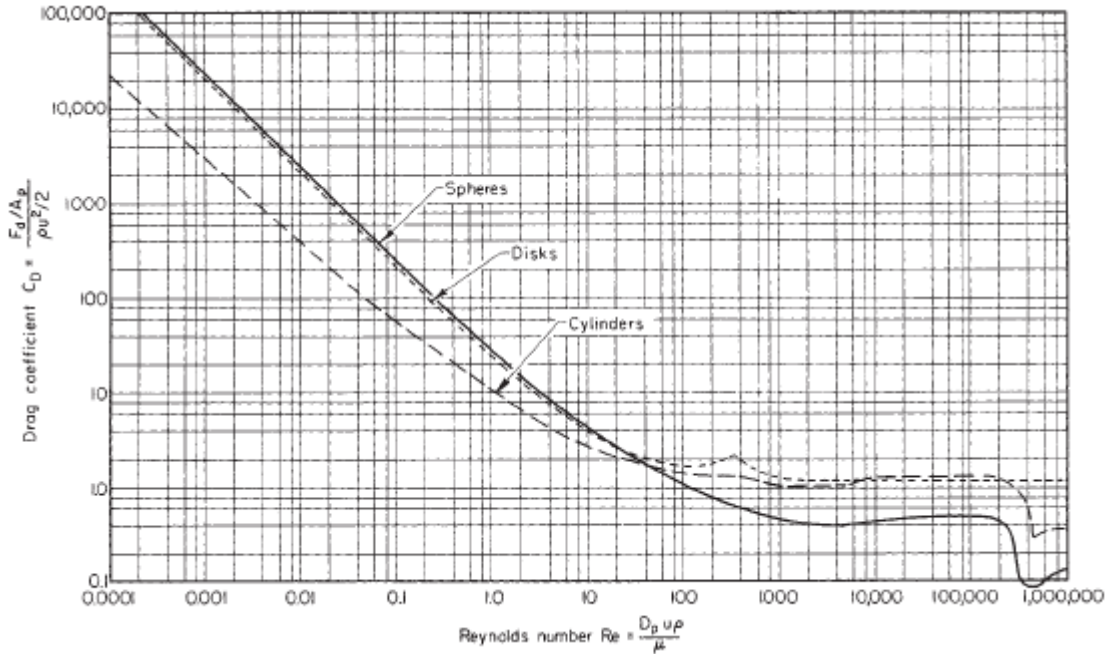

Figure 2-4. Drag coefficients for spheres, disks, and cylinders: A_p = area of particle projected on plane normal to direction of motion; C_D = overall drag coefficient, dimensionless; D_p = diameter of particle; F_d = drag or resistance to motion of body in fluid; Re = Reynolds number, dimensionless; u = relative velocity between particle and main body of fluid; μ = fluid viscosity; and ρ = fluid density. (Reprinted from Ref. 24. Copyright 1940 American Chemical Society).

Equation (41) describes the inertial drag force acting across individual debris elements contained within the bed. It is intuitively obvious that drag must be exerted along the surface of the debris; so many similarities arise with the previous treatment of viscous shear coupled to the walls of a flow channel. It was shown in Section 2.1.3.1 how viscous shear imparts a component of drag to the surface, so simple addition of an inertial drag term will duplicate this component. Nevertheless, the standard treatment is to define an inertia-induced drag stress analogous to Eq. (19) such that

$$\tau_{Drag} = \frac{F_D}{A_p} = \frac{R}{2}\left(\frac{dP}{dz}\right)_{Drag} . \tag{43}$$

One important question that immediately arises is, what area A_p should be used to distribute the drag force? Viscous shear was implicitly assumed through the application of hydraulic scaling factors to affect the entire surface of the debris. This might be reasonable for low-velocity flow that follows laminar streamlines around the contours of the obstacles, but for higher velocities approaching a turbulence transition, the flow will separate from the surface creating lee-wake eddies that do not feel the effects of drag. Figure 2-4 illustrates that this flow transition, marked by the flattening drag coefficients, does not occur until Re_p approaches or exceeds a value of 100 depending on the shape of the debris elements, so for now, it is reasonable to assume that inertial drag can also be distributed across the entire debris surface for the flow regimes of interest and introduce an empirical fitting constant to determine the best value supported by data.

Reversing the sign of Eq. (41) to account for inertial drag acting on a fluid element, substitution into Eq. (43), and solving for the pressure gradient leads to the relation

$$-\left(\frac{dP}{dz}\right)_{Drag} = \frac{1}{8} C_D\left(Re\right)\left(\frac{1-\varepsilon}{\varepsilon^3}\right) S_V \rho w_A^2 \tag{44}$$

where Eq. (31) was substituted for the hydraulic radius and the local flow velocity was expressed in terms of the approach velocity. By definition, this component of pressure drop is fully coupled to the debris elements and will contribute directly to bed compression. Comparison of this result to the second term of the Ergun correlation recast as Eq. (34) shows the form to be similar.

Only the choice of the drag coefficient in Eq. (44) remains to be rationalized. The Ergun coefficient for the quadratic term has a numeric value of approximately 0.3, which was derived from statistical fits to a wide variety of data for gas flow through packed beds at much higher Re_p than are typically of interest for sump-screen blockage. The corresponding value of the drag coefficient $\left(C_D = 2.33\right)$ would lie at an approximate Re_p of 40 for spherical elements and irregular cylindrical elements (see Figure 2-4). This range exceeds the Reynolds numbers expected for sump-screen, so fits of the quadratic coefficient to sump-screen head-loss data should yield even smaller numeric values than the Ergun recommendation.

It is interesting to note that if the standard Stokes-limit drag coefficient of $C_D = 24/Re$ for spherical particles is substituted in Eq. (44) using the hydraulic radius as the length scale for *Re*, then the pressure gradient induced by drag in the viscous regime is estimated to be $-\left(\frac{dP}{dz}\right)_{Drag} = 3\frac{\left(1-\varepsilon\right)^2}{\varepsilon^3} S_V^2 \mu w_A$. This is only slightly different from the first-term magnitude of Eq. (32) that was derived for viscous shear acting throughout the flow. The exact numeric coefficient of 3 arises in the derivation of Stokes' drag law from the analytic treatment of normal pressure forces acting on the surface of a sphere. In the ideal cylindrical capillary, surface-normal pressure forces were not considered because

the velocity field is perfectly tangential, but this effect certainly *is* present in a complex debris bed with internal rotational flow patterns, so the coefficient of 2 derived for Eq. (32) may underestimate the total effect of viscous dissipation in a debris bed. However, the initial substitution is only valid when $Re_p = Re_f$, so the porosity for a realistic bed could just as easily have a value where the coefficient of 3 overestimates viscous dissipation.

The relationship elucidated above between the pressure gradients induced by viscous dissipation and by inertial transfer, or drag, suggests that a generic form of the drag coefficient like $C_D(Re) = f(Re)/Re + h(Re)$ can be substituted in Eq. (44) to satisfy both limits of physical behavior. In this expression, $f(Re)$ and $h(Re)$ are functions that control the relative contributions of viscosity and impaction to the total pressure gradient under a given flow condition. The proposed substitution leads to a simple summation of the gradients expressed in Eqs. (32) and (44) with the undetermined functions $f(Re)$ and $h(Re)$ serving as respective coefficients. The simplest and most common choice is to set $f(Re)$ and $h(Re)$ equal to constants that can be determined by correlation with data. The accuracy of this approach depends on the range of *Re* over which the correlation is performed. Low *Re* data will lead to a very small value of *h* and a characteristic value of *f*. High *Re* will influence the relative magnitude of the coefficients in the opposite manner.

Rao further emphasized the potential effect of the quadratic drag term (Ref. 43) by adopting the Ergun coefficients and explicitly evaluating a partial denominator at the minimum porosity of interest (Ref. 31). Reasoning that porosities may range from 0.65 to 1.0 for beds composed primarily of fiberglass, a factor of ε^{-2} was explicitly evaluated at the minimum of the range $\left(\varepsilon^{-2} = 0.65^{-2} = 2.3\right)$ and applied to the recommended scalar coefficient to obtain an inertial drag term of the form $\left(\frac{dP}{dz}\right)_{drag} = 0.66\left(\frac{1-\varepsilon}{\varepsilon}\right) S_V \rho w_A^2$. This term, presented as part of the NUREG/CR-6224 head-loss correlation, has caused much controversy because by visual appearance it does not conform to the classical derivation presented above. However, by explicitly evaluating the minimum expected porosity, the equation does bound the functional behavior of the Ergun formula over the range of $0.65 \le \varepsilon \le 1.0$. Difficulties may arise when using the cited correlation to infer debris-bed properties from high-velocity head-loss data, because the porosity has already been artificially suppressed, but this is seldom a concern when testing in the velocity range of expected sump-screen applications because the inertial head-loss contribution is very small anyway.

In the range of very low velocities and correspondingly low *Re* appropriate for modern recirculation sump strainers, it will be sufficient to admit an unknown constant fitting coefficient, $h(Re) = h$, for the inertial pressure loss term. Figure 2-4 suggests a more accurate correction for the drag coefficient of the viscous term. In the viscous regime for $Re < 1$, the drag coefficient should trend as a straight line on a log-log plot.

This behavior indicates an underlying power law of the form $y = bx^m$, where m is the slope in log-log space and b is the log-log intercept where $\log_{10} Re = 0$, or $Re = 1$. (The form $y = bx^m$ expands to $\log_{10} y = m \log_{10} x + \log_{10} b$, which explains the linear plot on log-log axes). Thus, the viscous term of the drag coefficient should obey $f(Re)/Re = bRe^m$ and thus a suitable coefficient would be $f(Re) = bRe^{m+1}$.

Substitution of the generic drag coefficient $C_D(Re) = f(Re)/Re + h(Re)$ into Eq. (44) using the coefficients defined above and the hydraulic radius as the characteristic length of Reynolds number, $Re = \frac{\rho \bar{w} R_H}{\mu} = \frac{\rho w_A}{\mu(1-\varepsilon)S_V}\frac{\varepsilon}{\varepsilon}$, gives a composite pressure gradient including both shear and drag as

$$-\left(\frac{dP}{dz}\right)_{Drag+Shear} = \frac{b}{8}\frac{(1-\varepsilon)^2}{\varepsilon^3} S_V^2 \mu w_A Re^{m+1} + \frac{h}{8}\frac{(1-\varepsilon)}{\varepsilon^3} S_V \rho w_A^2 \tag{45}$$

where the first term of Eq. (45) is analogous to the first term of Eq. (32). From Figure 2-4, the log-log intercept for various shapes of debris element is in the range of $10 \le b \le 30$, so the leading constant should have a value in the range of 1 to 4, spanning the theoretical values of 2 - 3. If the theory of viscous pressure drop is perfectly accurate, the exponent fitting parameter will have a value near $m = -1$, meaning that no correction is needed. Similarly, if the theory for inertial drag is perfectly accurate then the fitting parameter will have a value near $h = 1$. Note that the correction factor $f(Re) = bRe^{m+1}$ should be applied to all terms of Eq. (32) for completeness.

At this point it is worth remembering that porosity and specific surface area are intended to be functions of spatial location in the debris bed. This means that the local Reynolds number is also a function of z. However, the fitting parameters b and m apply across the entire range of local flow conditions and should be relatively robust over a wide range of debris combinations. Note that Figure 2-4 presents variations in drag for particular shapes of debris elements as a function of their respective particle Reynolds number definitions. Analogous plots using the hydraulic radius should exhibit less variation because it subsumes all conditions of porosity and specific surface area.

2.1.4 Remaining Pressure Gradient Contributions

Recall that in Section 2.1.1.3.1 all terms of the force balance acting on a CV of water were grouped into additive components of the total pressure gradient. Viscous shear and inertial drag have been treated thus far, but extra terms grouped as $(dP/dz)_{Other}$ remain for consideration. Aside from the gravity force, which leads to increasing static pressure in a vertical bed, these terms arise from the initial presumption that spatial gradients exist in all physical variables. Equation (16c) can be scaled from a single capillary to a full debris bed using substitutions for flow area and hydraulic radius presented above. The simplified result is

$$-\left(\frac{dP}{dz}\right)_{Other} = \frac{2}{\varepsilon}\left(P + \frac{\beta}{\varepsilon^2}\rho w_A^2\right)\left[\left(\frac{1}{1-\varepsilon}\right)\frac{d\varepsilon}{dz} - \frac{\varepsilon}{S_V}\frac{dS_V}{dz}\right] + \frac{1}{\varepsilon^2}\rho w_A^2\frac{d\beta}{dz} - \rho g \tag{46}$$

Again, the net pressure change across the entire bed caused by internal gradients is zero because the flow attains the same conditions above and below the bed. Static pressure increases through the bed, but does not represent a characteristic head-loss induced by the debris. Static pressure difference is usually discarded during measurement by setting a zero differential between pressure transducers under zero flow with no debris present.

The most surprising feature of Eq. (46) is the explicit dependence on absolute local pressure $P(z)$. Formulas for net pressure change across a debris bed always treat pressure difference in a relative sense that is presumed to be constant regardless of the absolute inlet and outlet pressures. This term arises from the presumption that a spatial pressure gradient exists in combination with a changing local flow area. It should not be unexpected that solving for the internal profile of pressure gradient requires that the internal pressure distribution be known as well. For a configuration with fully specified spatial gradients of porosity and specific surface area, all coefficients could be quantified and the remaining differential equation for pressure could be solved by integration. Although pressure measurements typically reference upper and lower transducers to a common zero reference, it should not be difficult to calibrate one of the units to read absolute local pressure. Absolute inlet and outlet pressure measurements may be needed for future work that estimates bed compression and compaction effects using internal pressure gradient as a local driving force.

2.1.5 Summary of Head-Loss Gradient Formulas

Much has been learned about the origins of the linear and quadratic head-loss terms that appear in traditional correlations. The linear term represents viscous dissipation in the interstitial flow, and the quadratic term represents direct inertial transfer from the fluid to the debris elements. However, a satisfactory joint derivation of the two limiting behaviors has not been provided. This should not be too disconcerting given the somewhat broad abstraction of hydraulic similitude that was used to bridge the gap between theoretical formulas developed for ideal flow paths and the physical behavior of complex composite debris beds. It is more valuable to note that two theoretical limits are available to constrain empirical correlations that may be developed to describe a wide range of flow velocities and to adopt the standard approximation that total pressure drop can be expressed as a linear combination of several effects.

Several relationships that have been used frequently are repeated here for convenient reference:

Bulk Flow $$Q = \bar{w}A = \frac{w_A}{\varepsilon}\pi R^2; \tag{47a}$$

Hydraulic Radius $$R_H = \frac{R}{2} = \frac{\varepsilon}{(1-\varepsilon)S_V}; \tag{47b}$$

Reynolds Number $$Re = \frac{\rho w_A}{\mu(1-\varepsilon)S_V}. \tag{47c}$$

The total pressure gradient at any location z was expressed in Eq. (14) as

$$\boxed{-\left(\frac{dP}{dz}\right)_{Total} = -\left(\frac{dP}{dz}\right)_{Shear} - \left(\frac{dP}{dz}\right)_{Drag} - \left(\frac{dP}{dz}\right)_{Other}}. \tag{48}$$

Components of the total positive pressure *drop* can be summarized by collecting Eqs. (32), (44), and (46):

$$\boxed{-\left(\frac{dP}{dz}\right)_{Shear} = 2\frac{(1-\varepsilon)^2}{\varepsilon^3}S_V^2\mu w_A + \frac{16\beta}{3}\left(\frac{1-\varepsilon}{\varepsilon^3}\right)\left[\frac{\varepsilon}{(1-\varepsilon)S_V^2}\frac{dS_V}{dz} - \frac{1}{S_V(1-\varepsilon)^2}\frac{d\varepsilon}{dz}\right]S_V\rho w_A^2}; \tag{49}$$

$$\boxed{-\left(\frac{dP}{dz}\right)_{Drag} = \frac{1}{8}C_D(Re)\left(\frac{1-\varepsilon}{\varepsilon^3}\right)S_V\rho w_A^2}; \tag{50}$$

$$\boxed{-\left(\frac{dP}{dz}\right)_{Other} = \frac{2}{\varepsilon}\left(P + \frac{\beta}{\varepsilon^2}\rho w_A^2\right)\left[\left(\frac{1}{1-\varepsilon}\right)\frac{d\varepsilon}{dz} - \frac{\varepsilon}{S_V}\frac{dS_V}{dz}\right] + \frac{1}{\varepsilon^2}\rho w_A^2\frac{d\beta}{dz} - \rho g}. \tag{51}$$

Most applications involving reduction of pressure measurements taken across a debris bed will require integrated versions of the pressure drop components. For consistency, each component of positive pressure drop is defined as $-(P_{bot} - P_{top}) \equiv \Delta P$. The following condensed form assumes that flow conditions of velocity, porosity, and specific surface area are identical at the locations of the pressure taps:

$$\boxed{\Delta P_{Shear} = 2\mu w_A \int_{top}^{bot} S_V^2 \frac{(1-\varepsilon)^2}{\varepsilon^3} dz}. \tag{52}$$

3 Conclusion

Significant work remains to couple formulas derived here for differential pressure gradient to a continuum mechanics model of fiber bed compression, but the theory is now in place to support a description of nonuniform bed response. More challenging still is the development of a predictive model for bed compaction. As defined at the outset of this treatise, compaction involves the relative motion of individual debris elements. A complete description of controlling phenomena would include filtration mechanisms such as van der Waals attraction, momentum driven impaction, geometric sieving, migration, and eventual shedding from the debris bed. Some important steps have recently been taken to describe the macroscopic behavior of composite debris beds that will provide bounding constraints on microscopic predictive models (Ref. 46), but the micromechanics of bed response remain open to a fundamental description of motion induced by local pressure differences.

The greater value of a theoretical review of familiar topics like debris-bed head loss is often found in the fresh interpretation of data that is offered rather than in a fundamentally new predictive capability. This exercise has brought a renewed emphasis on the configurational aspects of bed formation, both from the perspective of composite structure and from the perspective of individual debris elements. New correlation groups have been proposed that offer a more explicit representation of surface roughness, tortuosity, and porosity as functions of location in the bed. These groups also support a new perspective of the relative importance between linear and quadratic terms of the classic head-loss equation as they pertain to the specific flow conditions and debris compositions experienced by modern sump strainers. As testing for the STP risk-informed closure project proceeds, it is hoped that this theory will be exercised and expanded to provide robust correlations for a wide parameter space of temperature, flow rate, particulate-to-fiber ratio, and fiber debris preparation.

4 BIBLIOGRAPHY

1. S. G. Ashbaugh and D. V. Rao, "GSI-191 Technical Assessment: Development of Debris Transport Fractions in Support of the Parametric Evaluation," U. S. Nuclear Regulatory Commission, NUREG/CR-6762, Vol. 4, Los Alamos National Laboratory, LA-UR-01-5965 (August 2002).
2. N. Ahmed, and D. K. Sunada, "Nonlinear Flow in Porous Media," Journal of the Hydraulics Division, Proceedings of the ASCE, HY 6, pp. 1847 -- 1857 (November 1969).
3. T. S. Andreychek, "Test Plan: Characterization of Chemical and Corrosion Effects Potentially Occurring Inside a PWR Containment Following a LOCA," Westinghouse Electric Company, LLC, Rev. 13 (July 20, 2005).
4. P. A. Baron and K. Willeke, "Gas and Particle Motion," in Aerosol Measurement: Principles, Techniques, and Applications, 2nd ed., Baron and Willeke editors, John Wiley and Sons, Inc. (2001).
5. J. Dallman, et. al., "Integrated Chemical Effects Test Project: Test #1 Data Report," U. S. Nuclear Regulatory Commission, NUREG/CR-6914, Vol. 2, Los Alamos National Laboratory, LA-UR-05-0124 (June 2005).
6. J. Dallman, et. al., "Integrated Chemical Effects Test Project: Test #2 Data Report," U. S. Nuclear Regulatory Commission, NUREG/CR-6914, Vol. 3, Los Alamos National Laboratory, LA-UR-05-6146 (September 2005).
7. J. Dallman, et. al., "Integrated Chemical Effects Test Project: Test #3 Data Report," U. S. Nuclear Regulatory Commission, NUREG/CR-6914, Vol. 4, Los Alamos National Laboratory, LA-UR-05-6996 (October 2005).
8. J. Dallman, et. al., "Integrated Chemical Effects Test Project: Test #4 Data Report," U. S. Nuclear Regulatory Commission, NUREG/CR-6914, Vol. 5, Los Alamos National Laboratory, LA-UR-05-8735 (November 2005).
9. J. Dallman, et. al., "Integrated Chemical Effects Test Project: Test #5 Data Report," U. S. Nuclear Regulatory Commission, NUREG/CR-6914, Vol. 6, Los Alamos National Laboratory, LA-UR-05-9177 (January 2006).
10. C. N. Davies, "The Separation of Airborne Dust and Particles," Proc., Inst. Mech. Eng. (London) B1, pp. 185 -- 198 (1952).
11. M. Ding, et. al., "Characterization and Head-Loss Testing of Latent Debris from Pressurized-Water-Reactor Containment Buildings," U. S. Nuclear Regulatory Commission, NUREG/CR-6877, Los Alamos National Laboratory, LA-UR-04-3970, (July 2005).
12. S. Ergun, "Fluid Flow through Packed Columns," Chemical Engineering Progress, Vol. 48, No. 2, pp. 89-94 (February 1952).

13. R. W. Fox and A. T. MacDonald, Introduction to Fluid Mechanics, Third Ed., John Wiley and Sons, Inc. (1985).

14. A. H. Harvey, A. P. Peskin, and S. A. Klein, "NIST/ASME Steam Properties: Formulation for General and Scientific Use – Version 2.11," U.S. Secretary of Commerce (1996).

15. W. C. Hinds, Aerosol Technology: Properties, Behavior, and Measurement of Airborne Particles, John Wiley and Sons, Inc. (1982).

16. W. L. Ingmanson, B. D. Andrews, and R. C. Johnson, "Internal Pressure Distributions in Compressible Mats under Fluid Stress," TAPPI, Vol. 42, No. 10, p. 840 (October 1959).

17. R. C. Johns, et. al., "Small-Scale Experiments: Effects of Chemical Reactions on Debris-Bed Head Loss," U. S. Nuclear Regulatory Commission, NUREG/CR-6868, Los Alamos National Laboratory, LA-UR-03-6415 (October 2003)

18. K. A. Jönsson, and B. T. L. Jönsson, "Fluid Flow in Compressible Porous Media: I. Steady-State Conditions," AIChE Journal, Vol. 38, No. 9, p. 1340 (September 1992).

19. K. A. Jönsson, and B. T. L. Jönsson, "Fluid Flow in Compressible Porous Media: II. Dynamic Behavior," AIChE Journal, Vol. 38, No. 9, p. 1349 (September 1992).

20. M. Kataja, A. Rybin, and J. Timonen, "Permeability of highly compressible porous medium," J. Appl. Phys. Vol. 72, No. 4, p.1271 (August 1992).

21. G. F. Knoll, Radiation Detection and Measurement, John Wiley and Sons, Inc., pp. 131-139 (1979).

22. E. Kreyszig, Advanced Engineering Mathematics, John Wiley and Sons, Inc., 7th ed., (1993).

23. C. P. Kyan, D. T. Wasan, and R. C. Kintner, "Flow of Single-Phase Fluids through Fibrous Beds," Ind. Eng. Chem. Fundam., Vol. 9, No. 4, pp. 596 -- 603 (1970).

24. Lapple and Shepherd, Ind. Eng. Chem., Vol. 32, 605 (1940).

25. B. C. Letellier, "Bayesian Methods for Inferring Soil Contamination Profiles from Neutron-Induced Gamma-Ray Spectra," Ph.D. dissertation, Kansas State University (1998).

26. R. D. Letterman, ed., Water Quality and Treatment, McGraw-Hill, Inc. 5th ed., pp. 337-341 (1999).

27. I. F. Macdonald, M. S. El-Sayed, K. Mow, and F. A. L, Dullien, "Flow through Porous Media—the Ergun Equation Revisited," Ind. Eng. Chem. Fundam., Vol. 18, No. 3, pp. 199-208 (1979).

28. D. C. Mays, and J. R. Hunt, "Hydrodynamic Aspects of Particle Clogging in Porous Media," Environ. Sci. Technol. Vol. 39, No. 2, pp. 577 -- 584 (2005).

29. R. H. Perry and D. W. Green, eds. Perry's Chemical Engineers' Handbook, 7th Ed., McGraw-Hill (1997).

30. D. V. Rao, C. J. Shaffer, and S. G. Ashbaugh, "GSI-191 Technical Assessment: Development of Debris Generation Quantities in Support of the Parametric Evaluation," U. S. Nuclear Regulatory Commission, NUREG/CR-6762, Vol. 3, Los Alamos National Laboratory, LA-UR-01-6640 (August 2002).

31. D. V. Rao, personal communication, October 2004.

32. W. A. Roesch, "The Effect of Post-LOCA Chemical Products on Pressurized Water Reactor Sump Screen Head Losses," Mechanical Engineering Master's Thesis, University of New Mexico, Albuquerque, New Mexico (May 2006).

33. Shaffer, et. al., "GSI-191: Experimental Studies of Loss-of-Coolant-Accident-Generated Debris Accumulation and Head Loss with Emphasis on the Effects of Calcium Silicate Insulation," U. S. Nuclear Regulatory Commission, NUREG/CR-6874, Los Alamos National Laboratory LA-UR-04-1227 (May 2005).

34. A. P. Sincero and G. A. Sincero, Physical-Chemical Treatment of Water and Wastewater, CRC Press, pp. 337-339 (2003).

35. U. S. NRC, "GSI-191 SE: Safety Evaluation of NEI Guidance on PWR Sump Performances, Appendix IV: Debris Transport Comparison," Rev. 0, ML043280641 (December 2004).

36. U. S. NRC, "Regulatory Guide 1.82: Water Sources for Long-Term Recirculation Cooling Following a Loss-of-Coolant Accident," Rev. 3, U. S. Nuclear Regulatory Commission (November 2003).

37. U. S. NRC, "GSI-191 SE: Safety Evaluation of NEI Guidance on PWR Sump Performances, Appendix II: Confirmatory Debris Generation Analyses," Rev. 0, ML043280641 (December 2004).

38. U. S. NRC, "Results of Chemical Effects Head Loss Tests in Simulated PWR Sump Pool Environment," IN-2005-26, U. S. Nuclear Regulatory Commission (September 2005).

39. L. H. Van Vlack, Elements of Materials Science and Engineering, Fourth Ed., Addison-Wesley Publishing Co., Inc., pp. 6-13, 192-194, 264-265 (November 1980).

40. W. A. Wallis, One-dimensional Two-phase Flow, McGraw-Hill, Inc. (1969).

41. F. White, Viscous Fluid Flow, McGraw-Hill, Inc. (1974).

42. D. Williams, J. Spangler, Physics for Science and Engineering, Litton Educational Publishing, Inc., pp. 251-257 (1981).

43. G. Zigler, J. Brideau, D. V. Rao, C. Shaffer, F. Souto, and W. Thomas, "Parametric Study of the Potential for BWR ECCS Strainer Blockage Due to LOCA Generated Debris," NUREG/CR-6224, prepared for the U. S. Nuclear

Regulatory Commission by Science and Engineering Associates, Inc. (October 1995).

44. K. Howe, "Summary of Chemical Effects Testing in 2012 for STP GSA-191 License Submittal," CHLE-015, University of New Mexico, January 21, 2013.

45. Nuclear Energy Institute (NEI). *ZOI Fibrous Debris Preparation: Processing, Storage, and Handling, Revision 1*, Jan 2012.

46. B. Letellier, "Parametric Model of Debris Penetration Through Sump Strainers With Concurrent Filtration and Shedding," LA-UR-13-20079, Los Alamos National Laboratory, January 2013.